



Submarine hydrothermal activity along the mid-Kermadec Arc, New Zealand: Large-scale effects on venting

C. E. J. de Ronde

GNS Science, P.O. Box 30-368, Lower Hutt, New Zealand (cornel.deronde@gns.cri.nz)

E. T. Baker

Pacific Marine Environmental Laboratory, National Oceanic and Atmospheric Administration, 7600 Sand Point Way NE, Building 3, Seattle, Washington 98115-6349, USA

G. J. Massoth

GNS Science, P.O. Box 30-368, Lower Hutt, New Zealand

J. E. Lupton

Pacific Marine Environmental Laboratory, National Oceanic and Atmospheric Administration, 2115 S.E. OSU Drive, Newport, Oregon 97365-5258, USA

I. C. Wright

National Institute of Water and Atmospheric Research, P.O. Box 14-901, Wellington, New Zealand

R. J. Sparks, S. C. Bannister, and M. E. Reyners

GNS Science, P.O. Box 30-368, Lower Hutt, New Zealand

S. L. Walker

Pacific Marine Environmental Laboratory, National Oceanic and Atmospheric Administration, 7600 Sand Point Way NE, Building 3, Seattle, Washington 98115-6349, USA

R. R. Greene

Pacific Marine Environmental Laboratory, National Oceanic and Atmospheric Administration, 2115 S.E. OSU Drive, Newport, Oregon 97365-5258, USA

J. Ishibashi

Faculty of Science, Kyushu University, 8128581 Fukuoka, Japan

K. Faure

GNS Science, P.O. Box 30-368, Lower Hutt, New Zealand

J. A. Resing and G. T. Lebon

Pacific Marine Environmental Laboratory, National Oceanic and Atmospheric Administration, 7600 Sand Point Way NE, Building 3, Seattle, Washington 98115-6349, USA

[1] The 2,500-km Kermadec-Tonga arc is the longest submarine arc on the planet. Here, we report on the second of a series of cruises designed to investigate large-scale controls on active hydrothermal venting on this arc. The 2002 NZAPLUME II cruise surveyed 12 submarine volcanic centers along ~580 km of the middle Kermadec arc (MKA), extending a 1999 cruise that surveyed 260 km of the southern Kermadec arc (SKA). Average spacing between volcanic centers increases northward from 30 km on backarc crust along

the SKA, to 45 km on backarc crust along the southern MKA, to 58 km where the MKA joins the Kermadec Ridge. Volcanic cones dominate in the backarc, and calderas dominate the Kermadec Ridge. The incidence of venting is higher along the MKA (83%, 10 of 12 volcanic centers) than the SKA (67%, 8 of 12), but the relative intensity of venting, as given by plume thickness, areal extent, and concentration of dissolved gases and ionic species, is generally weaker in the MKA. This pattern may reflect subduction of the ~17-km-thick oceanic Hikurangi Plateau beneath the SKA. Subduction of this basaltic mass should greatly increase fluid loss from the downgoing slab, initiating extensive melting in the upper mantle wedge and invigorating the hydrothermal systems of the SKA. Conversely, volcanic centers in the southern MKA are starved of magma replenishment and so their hydrothermal systems are waning. Farther north, where the MKA centers merge with the Kermadec Ridge, fewer but larger magma bodies accumulate in the thicker (older) crust, ensuring more widely separated, caldera-dominated volcanic centers.

Components: 19,542 words, 10 figures, 5 tables.

Keywords: submarine hydrothermal activity; mid-Kermadec Arc; New Zealand; venting.

Index Terms: 3017 Marine Geology and Geophysics: Hydrothermal systems (0450, 1034, 3616, 4832, 8135, 8424).

Received 29 September 2006; **Revised** 10 January 2007; **Accepted** 21 February 2007; **Published** 24 July 2007.

de Ronde, C. E. J., et al. (2007), Submarine hydrothermal activity along the mid-Kermadec Arc, New Zealand: Large-scale effects on venting, *Geochem. Geophys. Geosyst.*, 8, Q07007, doi:10.1029/2006GC001495.

1. Introduction

[2] Subduction zones ensure a steady supply of oceanic lithosphere that will undergo dehydration during the subduction process, releasing fluids into the overlying mantle wedge. These fluids trigger partial melting of the mantle wedge, in turn supplying melt to form magma bodies that underlie the volcanic centers along the active arc front. The longevity of hydrothermal systems associated with arc volcanoes, and even the intensity of their venting, is ultimately driven by the amount of heat extracted from these magma chambers. If the magma bodies can be replenished over time, then the hydrothermal systems will similarly be active for extended periods, an important condition in the formation of large mineral deposits.

[3] The Kermadec-Tonga arc forms part of the ~2,500-km-long, southward propagating and actively widening, Lau-Havre-Taupo arc-backarc complex associated with Pacific-Australian plate convergence (Figure 1). This complex is presently evolving from full oceanic spreading in the central and southern Lau Basin, through rifting of arc crust along the southernmost Lau and entire Havre Trough, to rifting within New Zealand continental crust [Gamble and Wright, 1995]. Flanking the Havre Trough, the remnant Colville Ridge (~5 Ma) and active (≤ 0.5 Ma) Kermadec arc margins form longitudinally continuous ridges, with the Hikurangi Plateau off the coast of East

Cape currently being subducted beneath the North Island of New Zealand. Volcanoes of the Tonga-Kermadec arc front occur within a 40 km wide zone that extends for the entire length of the Kermadec-Tonga arc, and which is populated by >45 volcanic centers (C. E. J. de Ronde et al., manuscript in preparation, 2007).

[4] The first systematic survey of an intraoceanic arc for hydrothermal venting occurred in 1999 when the NZAPLUME (New Zealand American PLUME Mapping Expedition) cruise mapped 13 volcanoes along 260 km of the southern Kermadec arc (SKA) and found 7 of them (55%) were active [de Ronde et al., 2001]. Incidence of venting along the active arc front was found to be similar to that of slow-to-medium spreading mid-ocean ridges (MORs) [Baker et al., 2003]. However, the concentration of certain chemical components within the arc hydrothermal emissions (plumes), such as CO₂, H₂S and Fe, were commonly many times enriched above those of MOR sites, and have been ascribed to input from magmatic sources [de Ronde et al., 2001; Massoth et al., 2003].

[5] Surveys of submarine volcanoes along the Kermadec arc and elsewhere, such as the Tofua [Stoffers et al., 2006] and Mariana arcs [Embley et al., 2006], have shown that hydrothermal activity is confined to the summits of the volcanoes with rare examples of discharge occurring down their flanks, typically within 400 m of the summit [de Ronde et al., 2003]. Nowhere has hydrothermal

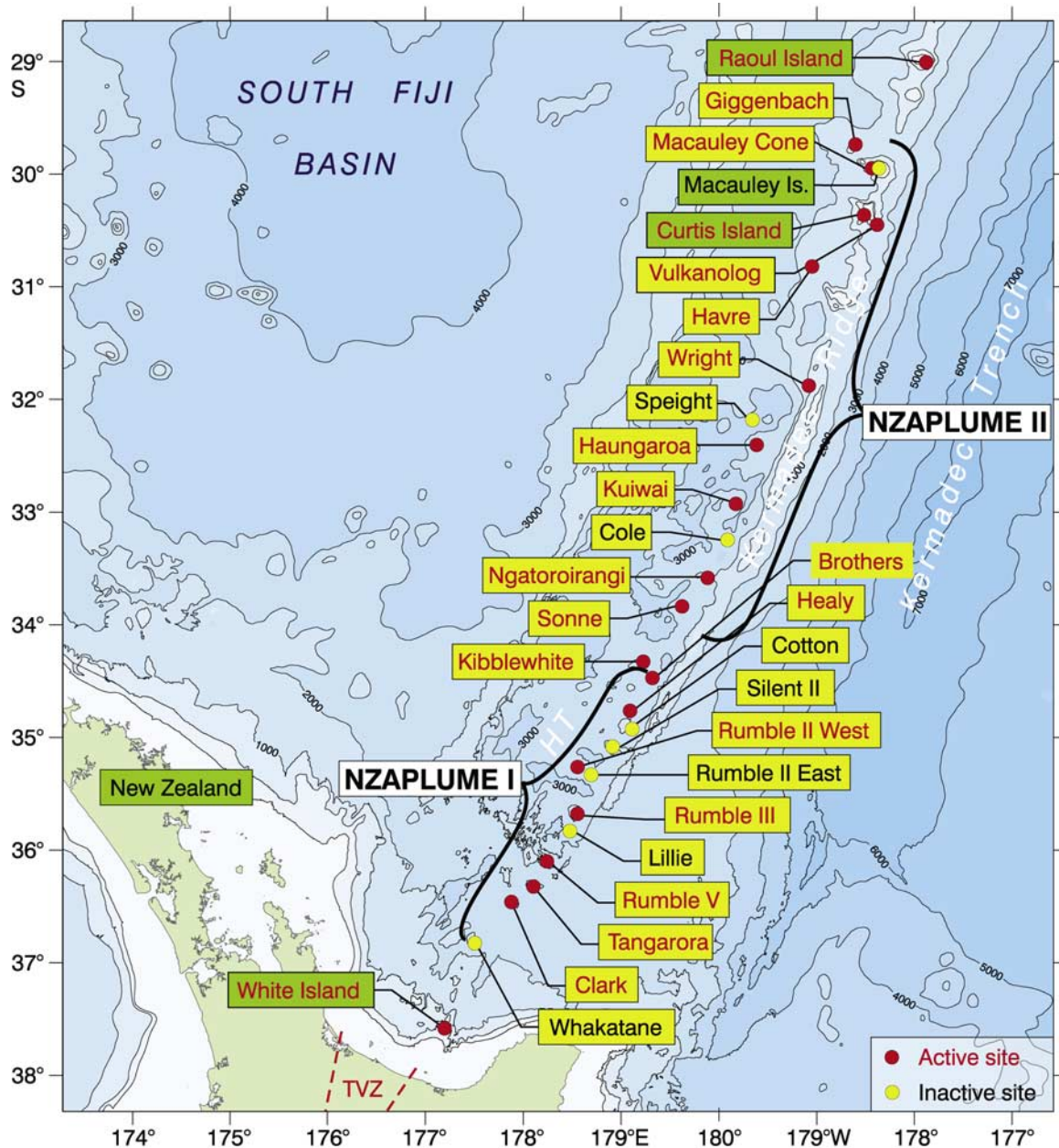


Figure 1. Location of the volcanic centers surveyed during NZAPLUME II (this work) and previously during NZAPLUME I [de Ronde et al., 2001]. Volcanically active White Island and Raoul Island bracket the dominantly submarine arc volcanoes of the Kermadec arc. Also shown for reference are the Cotton and Vulkanolog volcanic edifices reported by de Ronde et al. [2001] and mentioned in the text, but which are now considered part of the Healy and Curtis volcanic centers, respectively. In addition, Rumble II West and Rumble II East together now make up the Rumble II volcanic center. The vast majority of the volcanic centers along the Kermadec arc shown here are hydrothermally active (see legend), although activity is more subdued in the midpart of the arc (see text). HT, Havre Trough; TVZ, Taupo Volcanic Zone.

activity been detected on the seafloor between the volcanoes. Hydrothermal venting typically occurs in shallow-water to midwater depths, between ~1650 and 200 m [de Ronde et al., 2001; Baker et al., 2003], considerably shallower than those of

MORs (typically 2,200 to 2,600 m). Consequently, the maximum temperature of the expelled fluids will be less than those possible at MORs due to lower confining pressures of the overlying water column. This in turn enables processes such as



boiling, or phase separation, to occur more easily which can in turn enhance mineral deposition [Massoth *et al.*, 2003; de Ronde *et al.*, 2005].

[6] Since the first NZAPLUME cruise, additional expeditions have been staged with the aim of surveying the entire $\sim 2,500$ km of the Kermadec-Tonga arc for submarine hydrothermal emissions. Here, we report results of the 2002 NZAPLUME II cruise that investigated the next ~ 580 km of the middle Kermadec arc (MKA), NE from Brothers volcano (Figure 1). This study confirms that venting remains common along the arc, but that along-arc changes in tectonics and magma supply may control the relative intensity of hydrothermal venting.

2. NZAPLUME II

[7] The acquisition of additional bathymetric data along the Kermadec arc [e.g., Wright *et al.*, 2006] means we are now able to better define boundaries between segments along the arc. For example, here we define the southern boundary of the MKA as where a noticeable inflection in the slope of the seafloor occurs between the Kibblewhite and Sonne volcanic centers (around 34.1°S), where the seafloor flattens out (Figure 1 and see Figure 4 later). This is where the greatest depths to the seafloor occur along the arc front. The northern boundary of the MKA is defined as the northern margin of the northern-most (and largest) of the subaerial volcanic edifices along the arc, namely Raoul Island, for a total length of ~ 590 km. By contrast, the SKA encompasses all the volcanic centers south of Sonne to Whakatane (which marks the continental margin of New Zealand), now including Kibblewhite, a distance of ~ 360 km (i.e., an additional ~ 100 km longer than previously reported). The northern Kermadec arc (NKA) includes all those volcanic centers NE of Raoul Island up to the Monowai volcanic center for a total of 1,335 km for the entire Kermadec arc.

[8] The NZAPLUME II cruise of May 2002 surveyed 13 major volcanoes and 8 smaller volcanic edifices, together hosted by 12 volcanic centers of the MKA over 580 km, between Brothers and Giggenbach (Figure 1). The 105-km-long section between Giggenbach and Raoul Island was mapped during the September-October 2004 NZAPLUME III expedition with no vent sites found. Here, we define a volcanic center as being an assortment of volcanic edifices comprising a single large volcanic cone or caldera and/or groups of smaller (satellite) volcanoes with a minimum elevation of 500 m

above the seafloor, commonly separated from adjacent centers by several 10s of km. In this study they include, from south to north: Kibblewhite, Sonne, Ngatororangi, Cole, Kiuwai, Haungaroa, Speight, Wright, Havre, Curtis, Macauley and Giggenbach (Figure 1; Table 1). These names are the same as those used by Wright *et al.* [2006] for individual volcanoes, although where there is more than one volcano included in the center the name given here represents the most dominant edifice. The exceptions are the Cole, which was unnamed by Wright *et al.* [2006] (Figure 2), and Wright volcanic centers (Figure 3), the latter discovered along the arc front on a transit during the NZAPLUME III cruise. The volcanic centers of the MKA are located up to 42 km behind (west of) the Kermadec Ridge to sitting on the ridge itself (Figure 1). In addition, the Rapuhia volcanic center [Wright *et al.*, 2006] was also surveyed for hydrothermal plumes (none were found), although it is not considered to be part of the active arc front being located ~ 106 km behind the Kermadec Ridge (~ 53 km NW of Brothers volcano; not labeled in Figure 1), and thus is not discussed further in this paper. Finally, the 7 hydrothermally active volcanoes previously surveyed in 1999 along the SKA [de Ronde *et al.*, 2001] were revisited during NZAPLUME II. All of these volcanoes were still hydrothermally active in 2002 though they are not the focus of this paper.

2.1. Geology

[9] Depth to the seafloor along the NZAPLUME II survey, as determined by the basal depth of large volcanoes, starts at around 2,800 m just north of Brothers volcano, then becomes progressively deeper to reach 3,600 m immediately south of the Sonne volcanic center (Figure 4). Thereafter, it remains roughly at this depth for ~ 150 km until just south of the Haungaroa volcanic center whereupon the seafloor steadily shoals toward the Kermadec Islands where it is $\sim 1,300$ m deep near the Macauley volcanic center (Figure 4). The volcanic centers of Kibblewhite through Kiuwai clearly continue the trend of the arc front in the SKA, being located behind the Kermadec Ridge on back-arc crust, in this case by 21 to 41 km (Figure 1). By contrast, Haungaroa appears to be situated on a large pediment off the western flank of the ridge while the Wright volcanic center clearly sits on the ridge. In between, the Speight volcanic center is located 35 km behind the Kermadec Ridge although the seafloor ranges from a depth of ~ 2600 m around Speight volcano to 3,000 m around Oliver volcano situated a further



Table 1. Volcanic Centers of the Mid-Kermadec Arc

Name ^a	Latitude, °S	Longitude, °W/°E	Main Components ^b	Distance Between Centers, km ^c	Constructional Volume, ^d km ³	Number of Vent Sites	Location
<i>Southern Kermadec Arc</i>							
Kibblewhite	34 34.58	179 15.73E	dominant cone; 4 satellite cones	37 ^e	48	1	backarc
<i>Mid-Kermadec Arc</i>							
Sonne	34 04.62	179 34.53E	large caldera volcano	63	156	1	backarc
Ngatoroirangi	33 43.72	179 49.63E	large cone	45	217	1	backarc
Cole	33 24.57	179 52.29E	single cone	36	140	0	barkarc
Kuiwai	33 09.54	179 57.40W	large cone; satellite cone	32	158	1	backarc
Hungaroa	32 37.00	179 37.42W	large cone volcano	68	241	2	ridge
Speight	32 23.29	179 35.46W	two dominant cones	26	14	0	ridge
Wright	31 51.00	179 11.26W	dominant cones (2); satellite cones	71	57	1	ridge
Havre	31 06.50	179 02.45W	large caldera volcano	84	91	1	ridge
Curtis	30 32.25	178 33.25W	subaerial volcanic edifice	79	41	2 ^f	ridge
Macauley ^g	30 12.00	178 29.00W	large caldera volcano; satellite cones	38	269	3	ridge
Giggenbach	30 02.15	178 42.75W	dominant cone; 2 main satellite cones	31	36	1	ridge
Raoul	29 16.00	177 55.00W	large (subaerial) caldera volcano	116	160	1 ^h	ridge

^a Each volcanic center is named after the dominant volcanic edifice.

^b For further details of the volcanic edifices found within the volcanic centers, see *Wright et al.* [2006].

^c Distance is calculated between the summits of the dominant edifices and/or the actively venting volcano in the volcanic center; the total length between centers is not the same as a line between Brothers and Giggenbach volcanoes (580 km).

^d Calculated from terrain models of curved basal surfaces that enclose a polygon around the volcano isobaths which best represent the basal extent of the volcanic edifice for each center; the polygon is then digitized to form a 3-D surface which cuts through the base of the edifice (commonly inclined); volumes calculated using a GIS package of the edifice terrain model above the basal 3-D surface (modified after *Wright et al.* [2006]); Wright, Curtis, and Raoul estimates from swath mapping done during NZAPLUME III.

^e This is the distance between the Brothers and Kibblewhite volcanic centers (see Figure 1).

^f Includes the subaerial geothermal system on Curtis Island and the Vulkanolog submarine vent field ~19 km S of Curtis Island [*Gavrilenko, 1984; Stoffers et al., 1999*].

^g Centered on Macauley cone, just offshore (west) of Macauley Island.

^h Subaerial geothermal system on Raoul Island.

7.5 km to the west [*Wright et al., 2006*], suggesting this volcanic center impinges on the western-most margin of the Kermadec Ridge. We suggest therefore that the active arc front begins to intersect the western margin of the Kermadec Ridge near the Haungaroa volcanic center, around 32.6°S (Figure 1). Thereafter, the active arc front merges with the Kermadec Ridge until north of Raoul Island.

[10] Spacing of the volcanic centers is variable along the survey area and ranges from 26 km between Speight and Wright to 84 km between Wright and Havre, or 105 km if we include between Macauley and Raoul. There remains the possibility that the larger gaps could host additional volcanic centers that were not intersected during the survey, although with the exception of the section between Kibblewhite and Sonne (Table 1), the largest gaps all occur where the active arc front intersects the Kermadec Ridge (see below).

[11] The average spacing (i.e., the mean separation) between the volcanic centers Sonne and Raoul (our definition of the MKA) is 54 km (Table 1). If we

then examine the spacing of volcanic centers of the MKA that occur in the back-arc (i.e., Sonne to Haungaroa), the average spacing decreases to one center every 45 km. By contrast, the average spacing for volcanic centers that sit on, or in close proximity to the Kermadec Ridge (i.e., Haungaroa to Raoul), increases to one center every 58 km. For comparison, using the above definition of a volcanic center and applying it to the newly defined SKA (i.e., Whakatane, Clark, Tangarua, Rumble V, Rumble IV, Lille, Rumble III, Rumble II, Silent II, Healy, Brothers and now including Kibblewhite), the average spacing between these centers is 30 km.

[12] Volcanic centers of the MKA are commonly dominated by large, single volcanoes (Table 1). Cone-type volcanoes predominate where the arc front sits behind the ridge, a pattern also seen in the SKA, where only 3 of the 12 dominant volcanoes (Rumble II West, Healy and Brothers) have calderas (Figure 1). Caldera volcanoes are more common along the MKA where the arc front merges with the Kermadec Ridge. Satellite cones are found

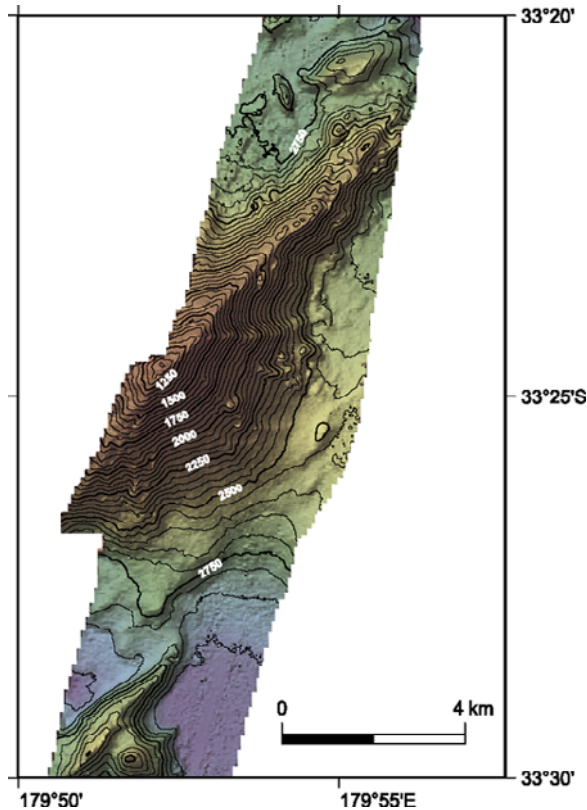


Figure 2. The Cole volcanic center is dominated by a single cone ~ 12 km long by up to ~ 6 km wide with an elevation of $\sim 1,400$ m off the surrounding seafloor and is located on the western margin of the Kermadec Ridge. The main edifice is elongated along a \sim NE-SW direction, similar to the regional structural fabric in the area. This map, together with that shown in Figure 3, complements those given by *Wright et al.* [2006] of volcanic centers of the MKA.

associated with some of the centers, notably at Kibblewhite, Kuiwai, Wright (see Figure 3), Macauley and Giggenbach, and are also seen further westward into the Havre Trough (Table 1) [see also *Wright et al.*, 2006]. Constructional volumes calculated for the dominant edifice at each volcanic center show that the cones range from 14 (Speight) to 241 km³ (Haungaroa) and the caldera volcanoes from 91 (Havre) to 269 km³ (Macauley; Table 1). While the largest cones are comparable in size to the largest calderas, on average they are about two thirds (67%) the constructional volumes (113 km³) of the caldera centers (169 km³). By contrast, using constructional volumes for SKA volcanic centers [*Wright et al.*, 2006] (less Whakatane but now including Kibblewhite), cones on average are similar in size to those of the MKA (100 km³) but calderas are much smaller, averaging 85 km³.

[13] Lavas recovered from volcanoes of the MKA have compositions dominated by basalt and basaltic andesite, with lesser amounts of dacite, and have been interpreted as forming a distinctly bimodal distribution [*Wright et al.*, 2006]. Caldera volcanoes such as Macauley and Havre are dominated by silicic lavas that have dacitic to rhyolitic compositions. Dacite is not restricted to the caldera volcanoes, however, having been recovered from Sonne and Giggenbach cones, although has not been recovered from the largest cone volcanoes along the MKA section (i.e., Ngatoroirangi, Kuiwai and Haungaroa). For further details on the geomorphology of the volcanic centers covered by the NZAPLUME II survey and geochemical analyses of rocks recovered from these localities, see *Wright et al.* [2006].

2.2. Hydrothermal Activity

[14] Hydrothermal plumes are the product of hydrothermal emissions that contain both particulate and dissolved chemical species. Thus, in order to best describe these plumes, we need tracers that correspond to both. Comparison of the distribution of different tracers along the 580-km-long transect between Kibblewhite and Giggenbach volcanoes is used to corroborate the source of the plumes, but also allows differences to be highlighted. Detailed conductivity-temperature-depth-optical (CTDO) surveys were done over all the major volcanoes along the MKA, in addition to single casts in between the volcanic centers (Figure 4). The major volcanoes of the SKA were also resurveyed for their hydrothermal emissions, with some of the results discussed elsewhere [e.g., *de Ronde et al.*, 2005]. A total of 29 vertical stations and 9 tow-yos were completed over the MKA volcanoes, and 11 vertical stations in between the centers. The surveys collected hydrographic and optical data in real time, and also discreet water samples that were analyzed onboard, or in land-based laboratories, for pH, $\delta^3\text{He}$, CH₄, H₂S, total dissolved Fe (TDFe) and Mn (TDMn), and filtered for particulates which were analyzed by thin-film X-ray fluorescence for various elements (Table 2; Appendix A).

[15] Light back-scattering measurements provide continuous detection of the concentrations of suspended particles, or turbidity in the water column, and are a simple and reliable means to determine hydrothermal activity over submarine volcanoes [*Baker et al.*, 2003]. Except near sea-surface and seafloor boundaries, suspended particles are overwhelmingly precipitates of hydrothermal fluids

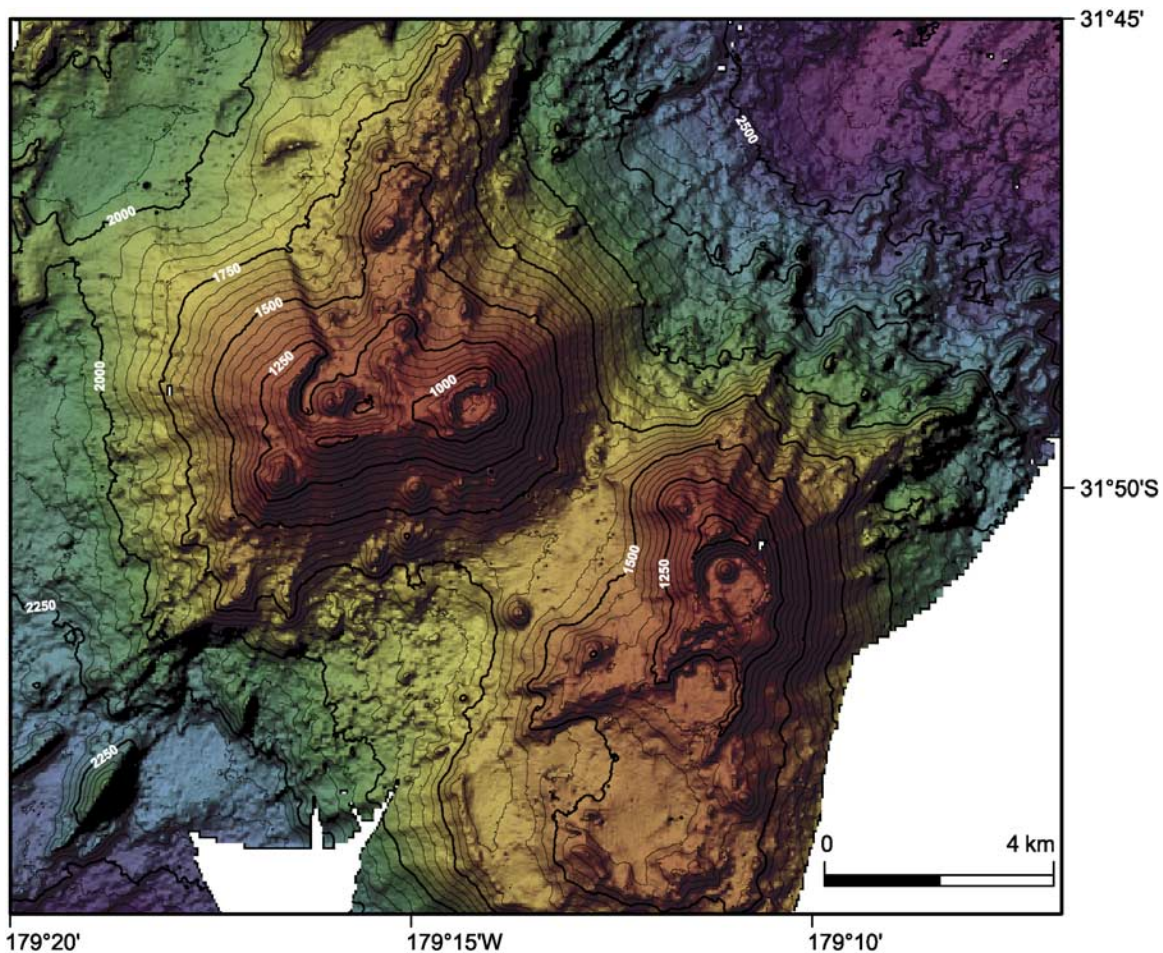


Figure 3. The Wright volcanic center is dominated by two large volcanic cones that each host two summit craters, with the largest 2 km across. A small cone rises out of one of the craters at each of the major volcanic edifices. This center also sits atop the Kermadec Ridge with each of the major cones having an elevation of at least 900 m above the seafloor. A CTDO tow-yo was done W-E over the summit of the western edifice and a single vertical cast in the center of the northern crater of the eastern edifice, where evidence for hydrothermal activity was noted. The dominant ~NE-SW structural grain of the regional fabric can be seen in the northern part of the map (compare to Cole volcano in Figure 2). This volcanic center was discovered during the 2004 NZAPLUME III cruise, which took a different route (i.e., more along the Kermadec Ridge) than that of the NZAPLUME II survey.

rich in dissolved iron and, especially along arcs, elemental sulfur. The thin (~200 m) surface layer of high particle concentrations shown in Figure 4a can be ascribed largely to organic and inorganic detritus. Concentrations decrease to a broad mid-depth minimum between ~700 m and 1600 m that grades into a thick bottom scattering layer below ~2,300 m down to the maximum depth sampled ($\geq 3,000$ m; Figure 4a). Superimposed on this background are hydrothermal plumes from nine of the volcanic centers: Kibblewhite, Sonne, Ngatoroirangi, Kuiwai, Haungaroa, Wright, Havre, Macauley and Giggenbach. Plumes at Wright, Giggenbach and Macauley were detected at least 5 km from their vent sources.

[16] Our plume studies also provide insight into the local distribution of vent sites, with some of the volcanic centers found to host more than one site. For example, Haungaroa appears to have a secondary vent field ~350 m down the flank of the main cone. And at least one, and possibly two other sources are thought to exist inside Macauley caldera that are not related to Macauley cone, itself located within the caldera [see *Wright et al.*, 2006]. Secondary sources for Havre and Macauley cone are more ambiguous. Havre may possibly have a second vent field around 1,505 m, or several smaller fields, although our results may indicate dilution of plumes with distance from a single source. Macauley cone has prominent plume max-

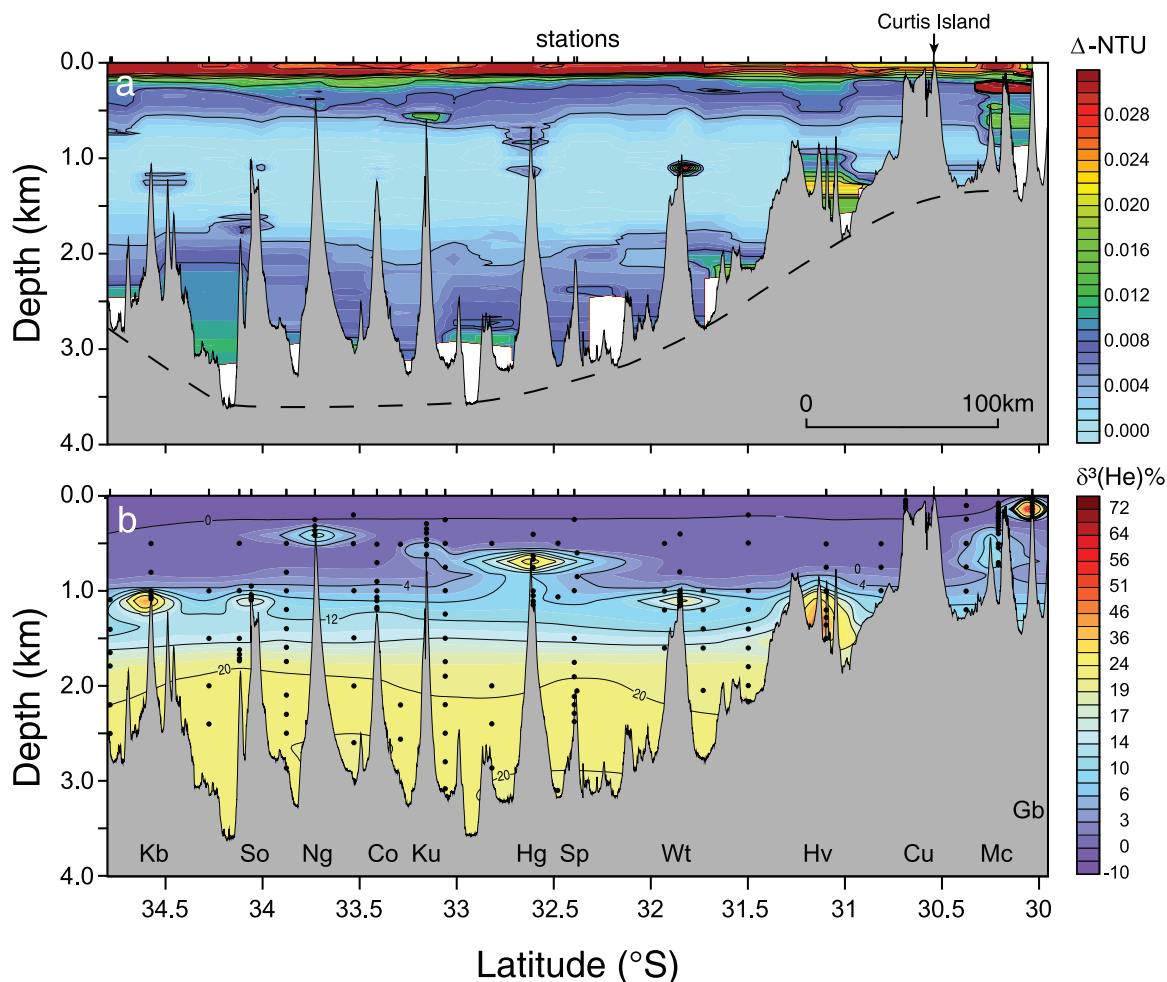


Figure 4. (a) Longitudinal section along the midpart of the Kermadec active arc front showing results of light-scattering data plotted as Δ -NTU (i.e., nephelometric turbidity units, a nondimensional optical standard). Vertical casts were conducted over the volcano summits and in between the volcanoes. In addition, deep tow-yo surveys were done over the Vulkanolog hydrothermal site (Curtis volcanic center), Macauley (cone), and Giggenbach and Wright volcanic centers, resulting in a much greater sample density over these volcanoes. Intense hydrothermal activity was easily distinguished by the light-scattering data above the Wright, Macauley, and Giggenbach centers with more diffuse activity noted over the volcanic centers farther south. Blank spaces in the figure denote areas of no data. Dashed line represents the depth to the seafloor, as determined by the basal depth of the major volcanoes. (b) Same section as in Figure 4a with discrete water sample locations given by the dots. The $\delta^3\text{He}$ values represent % increase in $^3\text{He}/^4\text{He}$ above air. Note that the contour interval is not constant in order to span the large dynamic range in the helium signal and that the gridding done in the plotting program artificially expands the horizontal extent of the plumes. The volcano shown depicting the Speight volcanic center is Oliver volcano [see Wright *et al.*, 2006]. Abbreviations: Kb, Kibblewhite; So, Sonne; Ng, Ngatoroirangi; Co, Cole; Ku, Kuiu; Hg, Haungaroa; Sp, Speight; Wt, Wright; Hv, Harve; Cu, Curtis; Mc, Macauley; Gb, Giggenbach.

ima at depths between 250 and 380 m that have most likely spread over this range as a result of mixing and/or variable depths of origin. Cole and Speight were the only volcanic centers that had no discernable light-scattering (or any other) anomalies.

[17] The Vulkanolog hydrothermal vent field is located \sim 19 km south of Curtis Island and is now considered to be part of the Curtis volcanic center. It

was discovered during an expedition in 1979 by the R/V *Vulkanolog* [Gavrilenko, 1984] and was later confirmed as still actively venting during a 1998 expedition by the R/V *Sonne* [Stoffers *et al.*, 1999]. However, tow-yo and single cast CTDO surveys conducted during NZAPLUME II failed to reveal any obvious light-scattering anomalies that could be ascribed to hydrothermal particulates, although



Table 2. Chemical Characteristics of Mid-Kermadec Arc Hydrothermal Plume Maxima^a

Volcano	Plume Depth, m	$\delta^3\text{He}$, ^b %	$\Delta^3\text{He}$, ^c %	ΔpH , ^d nM	CH_4 , ^e nM	TPS, ^f nM	VS, %	PCu, nM	PFe, nM	TDFe, ^g nM	TDMn, nM	Fe/Mn, ^h mol/mol	Fe/Mn, ⁱ mol/mol	R/R_A , ^j
Kibblewhite	1055	47	42	-0.03						23	22	1.0	1.5 ± 0.6	6.2
Sonne	1060	18	13	-						30	8	3.8	3.7 ± 0.4	-
Ngatoroirangi	415	14	14	-0.03						23	8	2.9		-
Kuiwai	615	6	5	-0.05						2	2	1.0		-
Hangaroa	670	36	35	-0.07						42	31	1.4	2.2 ± 0.8	7.0
	1000	11	7	-0.04						22	7	3.1	2.4 ± 0.5	-
Wright	1135	21	12	-	2.2	53	59	0.6	20	46	22	2.1	2.4 ± 0.4	-
Havre	1360	58	45	-		11	0	0.3	53	67	137	0.5	0.5 ± 0.1	-
Macauley														
Cone	310	15	15	-0.39	6.6	1725	78	0.9	3125	2600	303	8.6	9.1 ± 9.3	7.2
Caldera	525	8	7	-	2.1	3	0	0.1	15	23	4	5.8		-
	725	12	10		1.7					8	5	2.0		-
Giggenbach	120	65	65	-0.05	8.1	139	53	0.4	25	40	33	1.2	0.9 ± 0.5	7.2

^aDash (-), below detection (see below); blank space, not analyzed. NZAPLUME II particulate samples were not analyzed until a year after collection and may have lost some volatile sulfur. All the Wright samples were collected during the 2004 NZAPLUME III cruise, while some of the Macauley cone and Giggenbach samples were collected during the 2005 NZASRoF cruise. Discrete water samples were collected in custom fabricated Teflon-coated PVC bottles closed by silastic springs. Values reported in Table 2 represent samples with the highest concentrations for any one plume, except the Fe/Mn values shown with errors. Not all samples correspond to the same sampling bottle and exact tabulated depth, but rather represent maxima for an available data set for any one plume. Abbreviations: TPS, total particulate sulfur; VS, volatile sulfur (% of TPS lost under vacuum, dominantly native S); TDFe, total dissolvable Fe; TDMn, total dissolvable Mn; nM, nanomoles per L; mol, moles.

^b $\delta^3\text{He}$: Upon recovery of the CTD-rosette package, samples for helium analysis were immediately sealed into copper tubing using a hydraulic crimping device [Young and Lupton, 1983]. Helium concentrations and helium isotope ratios were determined using a 21-cm radius, dual collector mass spectrometer. The 1σ precision for the $^3\text{He}/^4\text{He}$ measurements is 0.2% in $\delta^3\text{He}$. Background $\delta^3\text{He}$ (%) values at 500, 1000, and 1500 m depth are $\sim 1.0\%$, $\sim 5.5\%$, and $\sim 15.0\%$, respectively; $\delta^3\text{He}$ values represent % increase in the value for $^3\text{He}/^4\text{He}$ above air ($\delta^3\text{He} = 100 [(R/R_A) - 1]$) and are the maximum values measured at that site.

^c $\Delta^3\text{He}$ refers to the difference between measured and background $\delta^3\text{He}$ values, which increase with depth.

^dpH was determined by a potentiometric combination electrode referenced to NBS standards at 25°C with an accuracy and precision of 0.01 and 0.005 pH units, respectively. ΔpH is the departure of a sample from the regional depth trend, determined with a precision of ≤ 0.01 pH units.

^e CH_4 was determined either using a combined automated purge and trap/gas chromatograph system [Ishibashi et al., 1997] or a head-space equilibration method [Faure et al., 2006]. Analytical reproducibilities are estimated at $\sim 5\%$ and 8% , respectively.

^fTPS, VS, and particulate Fe (PFe) and Cu (PCu) were determined by thin-film X-ray fluorescence on filters [Feely et al., 1991] (1σ 11% S-species, 2% Fe, 7% Cu).

^gTDFe and TDMn were determined on unfiltered samples acidified to pH 1.6 using kinetic-catalytic colorimetric methods adopted for flow-through injection analysis [Resing and Mottl, 1992; Measures et al., 1995] ($1\sigma \leq 6\%$ Mn, $\leq 8\%$ Fe). TD refers to dissolved plus freshly precipitated hydrothermal metal phases soluble in weak acid.

^hFe/Mn value based on plume concentration maxima; note the maxima for Mn and Fe are not everywhere from the same sample.

ⁱFe/Mn ratio based the mean and standard deviation for all enriched paired samples in that plume.

^j R/R_A , $R = (^3\text{He}/^4\text{He})_{\text{Sample}}$ and $R_A = (^3\text{He}/^4\text{He})_{\text{Air}}$; those sites with no reported R/R_A values had insufficient samples with high enough ^3He concentrations so that a linear regression fit to the data could be made to calculate the R/R_A value.

the very shallow nature of this site (110 m) means they would be difficult to discern from plankton and other near-surface sources of turbidity. Moreover, various chemical tracers (see below) did not indicate any hydrothermal discharge over the site, suggesting that this vent field may have ceased activity.

[18] Helium isotopes, available only after shore-based analysis, are an unambiguous indicator of hydrothermal input and thus provide confirmation of the hydrothermal origin of the particle plumes [Lupton, 2001]. They can also detect relatively weak hydrothermal emissions, such as diffuse venting, and discharge from predominantly gas-rich sources that are not easily discerned by light-scattering [de Ronde et al., 2001]. For samples such as volcanic rocks and

vent fluids that are highly enriched in helium, the helium isotope ratios are usually expressed as R/R_A where $R = (^3\text{He}/^4\text{He})_{\text{Sample}}$ and $R_A = (^3\text{He}/^4\text{He})_{\text{Air}}$. For our plume studies, these are estimates based on linear regression fits to water column ^3He and ^4He concentrations. The relatively small variations observed in the seawater samples (Table 2, Figure 4b) are expressed as $\delta^3\text{He}$ (%), the percentage deviation of the ratio in air, where $\delta^3\text{He} = 100 [(R/R_A) - 1]$. Plumes defined by $\delta^3\text{He}$ have a coarser resolution owing to their dependence on discrete samples, but nevertheless closely match the light-scattering results (compare Figure 4a with 4b). Sampled $\delta^3\text{He}$ maxima in the plumes range from 6% to 65%, with only Kibblewhite, Hangaroa, Havre and Giggenbach having values $>35\%$. However, even in the case of

the weakest light-scattering anomalies, such as those over Sonne and Ngatoroirangi, the $\delta^3\text{He}$ results confirmed that venting is indeed occurring at these sites. If the $\delta^3\text{He}$ maxima are corrected for their background values, which increase with depth, the same volcanoes still have the highest $\delta^3\text{He}$ concentrations (Table 2). $^3\text{He}/^4\text{He}$ values of the source fluids are about 6–7 \times higher than the same ratio in air, similar to those for plumes from the SKA [*de Ronde et al.*, 2003], and typical of fluids sampled from subaerial volcanoes and geothermal systems overlying subduction zones [*Hulston and Lupton*, 1996; *Patterson et al.*, 1997], but distinct from plumes venting along MORs ($R/R_{\text{Air}} = \sim 7.7\text{--}8.1$ [*Lupton*, 1998]).

[19] A notable regional feature is a maxima in $\delta^3\text{He}$ of $\geq 20\%$ extending throughout the area at depths between $\sim 1,900$ m down to around 3,000 m. This coincides with a thick bottom nepheloid layer that begins at $\sim 2,200$ m, extending down to the seafloor in the backarc part of the MKA (Figures 4a and 4b). This deep helium plume appears to be a continuation of a regional layer seen at similar depths along the northern portion of the SKA [*de Ronde et al.*, 2001]. Existing bathymetric maps show that a prominent sill separates the northern Havre Trough from the southern Lau Basin, precluding supply of ^3He -rich water by southward flow of deep hydrothermal plumes that might originate within the Lau Basin. Thus *de Ronde et al.* [2001] suggested that this deep layer might represent the distal part of the deep ($\sim 2,500$ m) hydrothermal helium signal originating near 15°S on the East Pacific Rise [*Lupton*, 2001]. However, bathymetric surveys undertaken during the 2004 NZAPLUME III cruise show that this sill does not exist thereby removing any impediment to a Lau Basin source. For further information on the data used to compile Figure 4b, and the methods used to obtain this data, see Appendix A, section A1.

[20] Diversity of the hydrothermal plumes associated with the MKA becomes more apparent if we examine their chemistry and other physical properties in detail. Measurement of pH is not a direct measure of dissolved gases although negative shifts in pH compared to the regional depth trend (ΔpH) are commonly interpreted as indicators of magmatic gas (e.g., CO_2 , SO_2 , H_2S) discharge [*Resing and Sansone*, 1996; *Resing et al.*, 2004]. The discharge of acids (e.g., H_2SO_4) may also be an important source of plume low pH values in arc environments [*Massoth et al.*, 2003; *de Ronde et al.*, 2005]. Values of ΔpH for the MKA vent sites were either

unmeasurable or relatively small, ranging from -0.03 to -0.07 . The one exception is the Macauley cone plume with a ΔpH value of -0.39 (Table 2).

[21] Methane is another geochemical tracer for volatile input [e.g., *Ishibashi et al.*, 1997] and was analyzed from plume samples collected over Wright, Macauley cone, Macauley caldera, and Giggenbach vent sites with concentration maxima ranging for the first three from 1.5 nM to 2.7 nM, to 8.1 nM for Giggenbach (Table 2). The lower values compare favorably with maxima from the cone and NW caldera sites at Brothers volcano of the SKA, which range between 1.4 and 4.0 nM [*de Ronde et al.*, 2005]. Gas discharge at Giggenbach may be relatively enriched in CH_4 considering the measured values, and the small shift in pH of -0.05 which would otherwise indicate high concentrations of CO_2 . Background CH_4 values for casts in between the volcanoes are < 1.0 nM.

[22] Hydrogen sulfide was not detected in any of the plume water samples (detection limit = 200 nM). However, submersible dives during April 2005 at Macauley cone (see <http://oceanexplorer.noaa.gov/explorations/05fire/>) showed this site was precipitating large amounts of elemental sulfur. Had plume samples been analyzed then, H_2S may well have been detected.

[23] Total dissolvable Fe (TDFe) and Mn (TDMn) represent the sum of dissolved and easily dissolvable (at pH 1.6) particulate Fe and Mn in the plume samples, respectively. These two metals are commonly major components in vent fluids, with concentrations that can exceed those of seawater by up to 10^6 and thus are also ideal tracers of hydrothermal discharge [*Massoth et al.*, 2003]. Iron and Mn anomalies were detected over all the hydrothermally active sites along the MKA (Table 2), consistent with the $\delta^3\text{He}$ and light-scattering results. Plume maxima for Fe concentrations are typically in the range 23–67 nM with a low value for Kuivai (2 nM) and a $1000\times$ higher value for the Macauley cone site (2,600 nM). Similarly, Mn concentrations mostly range between 7 and 33 nM with low values for Kuivai (2 nM) and Macauley caldera (4 nM), and high values for Havre (137 nM) and Macauley cone (303 nM). Background values for Fe and Mn concentration have been measured along the SKA as 2.5 ± 1.8 and 1.7 ± 0.8 nM, respectively [*Massoth et al.*, 2003], casting some doubt that Kuivai, in particular, has a Fe and/or Mn plume associated with venting (Table 2). Mean values of Fe/Mn are more easily compared between sites and are fairly consistent along the MKA, with the majority between

1.5 and 3.7. Only Macauley cone has a higher value at 9.1, while the plume from Havre had a ratio less than unity, at 0.5 (Table 2).

[24] Suspended particulate matter was collected from those plumes with the highest light-scattering anomalies by pressure filtration onto 0.4 μm polycarbonate filters and analyzed for total particulate sulfur (TPS), copper (PCu) and iron (PFe), among other elements, by thin-film energy dispersive X-ray fluorescence spectrometry [Feely *et al.*, 1991]. Elemental, or volatile sulfur (VS), was determined by the difference between TPS concentrations measured before and after evacuation of the sample chamber [Feely *et al.*, 1999], and is reported in Table 2 as a percentage of the TPS. Plume particulate S concentrations range from low at Macauley caldera (3 nM) to very high at Macauley cone (1,725 nM) with elemental sulfur dominating the samples from Wright, Macauley cone and Giggenbach, while undetected over the Havre and Macauley caldera sites. Particulate Fe concentrations are relatively low with only the Macauley cone plume (1,045 nM) of any significance. Particulate Cu concentrations ranged from 0.1 to 0.8 nM (Macauley cone), where analyzed (Table 2). See Appendix A, section A2, for further information on the methods used to acquire the particulate data, and the data used to compile Figure 7 (later).

[25] Comparison with particulate data for vent sites of the SKA [de Ronde *et al.*, 2001] shows TPS values are higher than those for the MKA, with the exception of Macauley cone. Elemental S in SKA plumes is either dominant (e.g., Rumble V and Brothers) or barely measurable (e.g., Rumble III and Healy), as at the MKA sites. Particulate Fe concentrations generally are higher for SKA sites with several having concentrations >300 nM with Brothers up to 1,213 nM, whereas particulate Cu is similar to MKA values at <0.9 nM, with the exception of Healy (1.3 nM) and Brothers (4.7 nM [de Ronde *et al.*, 2001, 2005; C. E. J. de Ronde, unpublished data, 2005]).

[26] Radiocarbon analysis was done on water samples ($n = 149$) collected from stations that spanned both the SKA and MKA, with the aim of: (1) measuring depth profiles for radiocarbon in the ocean north of New Zealand, (2) determining the distribution of inorganic carbon in the water column, and (3) detecting a carbon isotope signal in the water column near, or within, the hydrothermal plumes. Radiocarbon, like helium, also acts as a tracer for large-scale geostrophic flow. Profiles from 18 sampling stations are shown in Figures 5a and 6c.

The radiocarbon concentrations are expressed as $\Delta^{14}\text{C}$ (in ‰), which is defined as the $^{14}\text{C}/\text{C}_{\text{total}}$ value relative to the Modern Radiocarbon Standard ($^{14}\text{C}/\text{C}_{\text{total}} = 1.176 \times 10^{-12}$) after the sample stable carbon isotope ratio has been corrected to -25‰ , with mean errors of $\pm 4.3\text{‰}$.

[27] The general shape of the profiles is typical for the deep ocean in the Southern Hemisphere, with relatively higher values than those found in northern midlatitudes [e.g., Key, 2001]. All the profiles have higher $\Delta^{14}\text{C}$ values in near-surface water reflecting proximity to the atmospheric source. $\Delta^{14}\text{C}$ values down to -200‰ are more negative than those of Northern Hemisphere oceans, consistent with the average age of the Pacific Ocean water being relatively older than Atlantic or Indian Ocean water [Key, 2001]. The “in-between” station V02A-36 represents a typical deep water profile in the study region. Located south of Havre, it is the northern-most station for which ^{14}C data were obtained, and it shows the lowest $\Delta^{14}\text{C}$ values for all depths. By contrast, the profile at station V02A-52, located between Tangaroa and Clark, shows a discontinuity at about 800 m depth, representing a marked increase in $\Delta^{14}\text{C}$ relative to V02A-36 below 800 m down to $\sim 1,200$ m (Figure 5a). These two profiles define an envelope between which virtually all the $\Delta^{14}\text{C}$ points lie.

[28] Closer inspection of the data suggests there are further indications of anomalies relative to the general $\Delta^{14}\text{C}$ trend for individual casts. Notable in this regard are the vertical stations V02A-44 (inside Macauley caldera), V02A-37 (inside Havre caldera), V02A-19 (between Ngatoroiangi and Cole), V02A-06 (between Brothers and Kibblewhite) and V02A-04 (above the Brothers NW caldera site), and the tows T02A-13 (inside Healy caldera) and T02A-10 (inside Brothers caldera). These profiles show regions of very low (and on occasion high) $\Delta^{14}\text{C}$ gradient, which may indicate forced mixing in layers up to 500 m thick. It is not clear, however, whether such mixing would be thermally driven or the natural response to a homogenous body of water trapped within the calderas. A sample from V02A-44 that has a $\Delta^{14}\text{C}$ value $\sim 20\text{‰}$ lower than background is of a similar depth (400 m) to the main Macauley cone plumes within Macauley caldera (Table 2). The cast above Havre shows a marked change to lower $\Delta^{14}\text{C}$ values between 1,200 and 1,360 m inside the caldera where the hydrothermal plume maxima occurs at 1,360 m. Shifts away from the regional $\Delta^{14}\text{C}$ background begin at Brothers at 1,190 m continuing down to 1,440 m (V02A-04 and

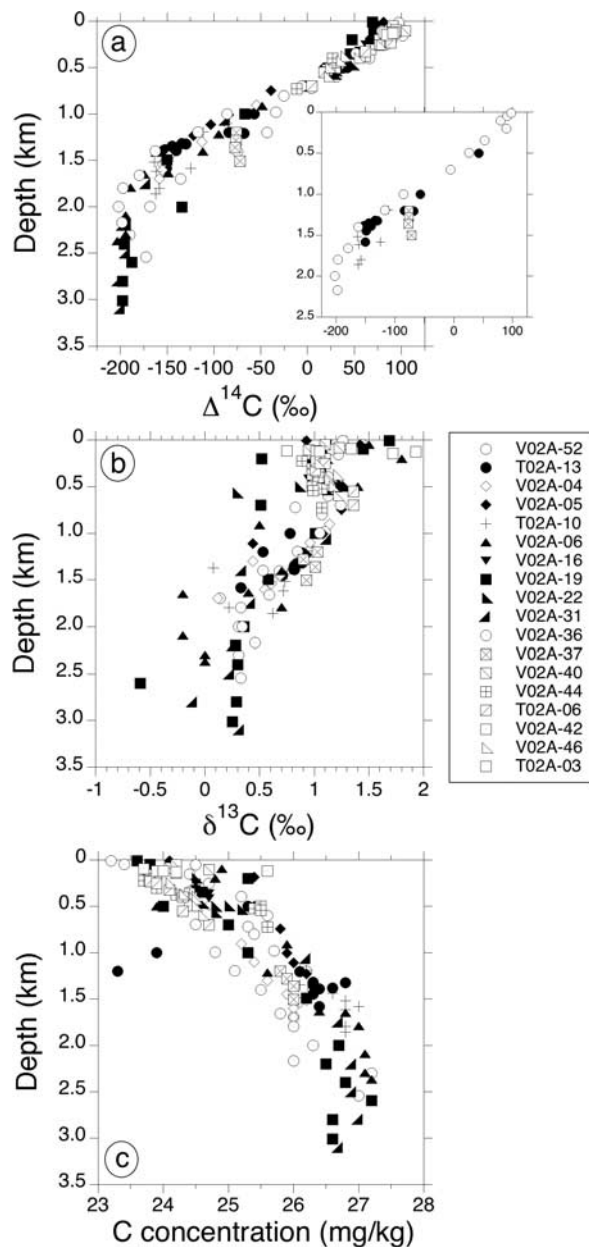


Figure 5. (a) Radiocarbon ($\Delta^{14}\text{C}$) profiles for various vertical (V) cast and tow-yo (T) CTDO surveys done over volcanic edifices of the mid-Kermadec arc. Inset: Evidence for mixing of ocean water within calderas is given by vertical trends in $\Delta^{14}\text{C}$ values for casts such as T02A-13 (Healy), T02A-10 (Brothers), and V02A-37 (Harve), when compared to a typical deep water profile in the study region (V02A-36; see text). (b) Carbon stable isotope ratios likely reflect the effects of biological activity in the water column. (c) Carbon yields show a relatively steady increase in carbon content with depth for individual casts.

T02A-10), similar to plume depths from the cone site (1,195–1,365 m). Thereafter, fairly uniform $\Delta^{14}\text{C}$ values occur between $\sim 1,520$ and 1,860 m, coincident with the caldera rim depth (1,540 m) with the NW caldera vent site located deeper within the caldera (Table 2) [see *de Ronde et al.*, 2005]. Similarly, deviation of $\Delta^{14}\text{C}$ values away from the regional trend at Healy (T02A-13) is noted in samples starting at $\sim 1,200$ m down to 1,390 whereupon the values are more homogeneous down to 1,580 m, coincident with hydrothermal venting associated with a small cone just outside (south of) the caldera (1,180 m) and the caldera rim (1,420 m), respectively [Baker *et al.*, 2003] (see inset to Figure 5a). There are no clear indications that primordial water depleted in ^{14}C is being injected in these regions. Thus we believe the simplest explanation for uniform $\Delta^{14}\text{C}$ values within the calderas is related to caldera filling processes. That is, water at the sill depth fills up the caldera so that the entire caldera has water with a $\Delta^{14}\text{C}$ value equal to that at the sill depth. Vertical mixing from venting may also play a role, although is probably less important than simple occasional spillover of denser water across the caldera rim.

[29] Those anomalies associated with “in-between” volcano casts that show deviations away from the regional trends are less obviously associated with hydrothermal venting, although station V02A-06 (between Brothers and Kibblewhite) has a normal $\Delta^{14}\text{C}$ profile to $\sim 1,500$ m whereupon there is a -30‰ shift that persists to a depth of 1,700 m (Figure 5a), coincident with the rim depth of Brothers volcano where hydrothermal plumes are known to escape into the surrounding ocean [Baker *et al.*, 2003]. At station V02A-19 (between Ngatoroangi and Cole) the sample collected at $\sim 2,000$ m is about 60‰ higher in $\Delta^{14}\text{C}$ than the regional value, and together with the anomalous deeper values north of Brothers, is coincident with a “deep” helium plume seen throughout the area [de Ronde *et al.*, 2001] (see Figure 4b). Overall, the trend is for deep water ($>1,800$ m) to show reduced ^{14}C content as the sampling stations approach the equator. This is in line with the trend associated with deep water circulation [Key, 2001].

[30] The stable isotope ratios through the water column, expressed as $\delta^{13}\text{C}$, are shown in Figure 5b and have errors of $\pm 0.1\text{‰}$. The data show some scatter, part of which may be instrumental, but nevertheless there is a coherent structure discernable in the profiles. Features include approximately constant $\delta^{13}\text{C}$ values down to 500 m, followed by

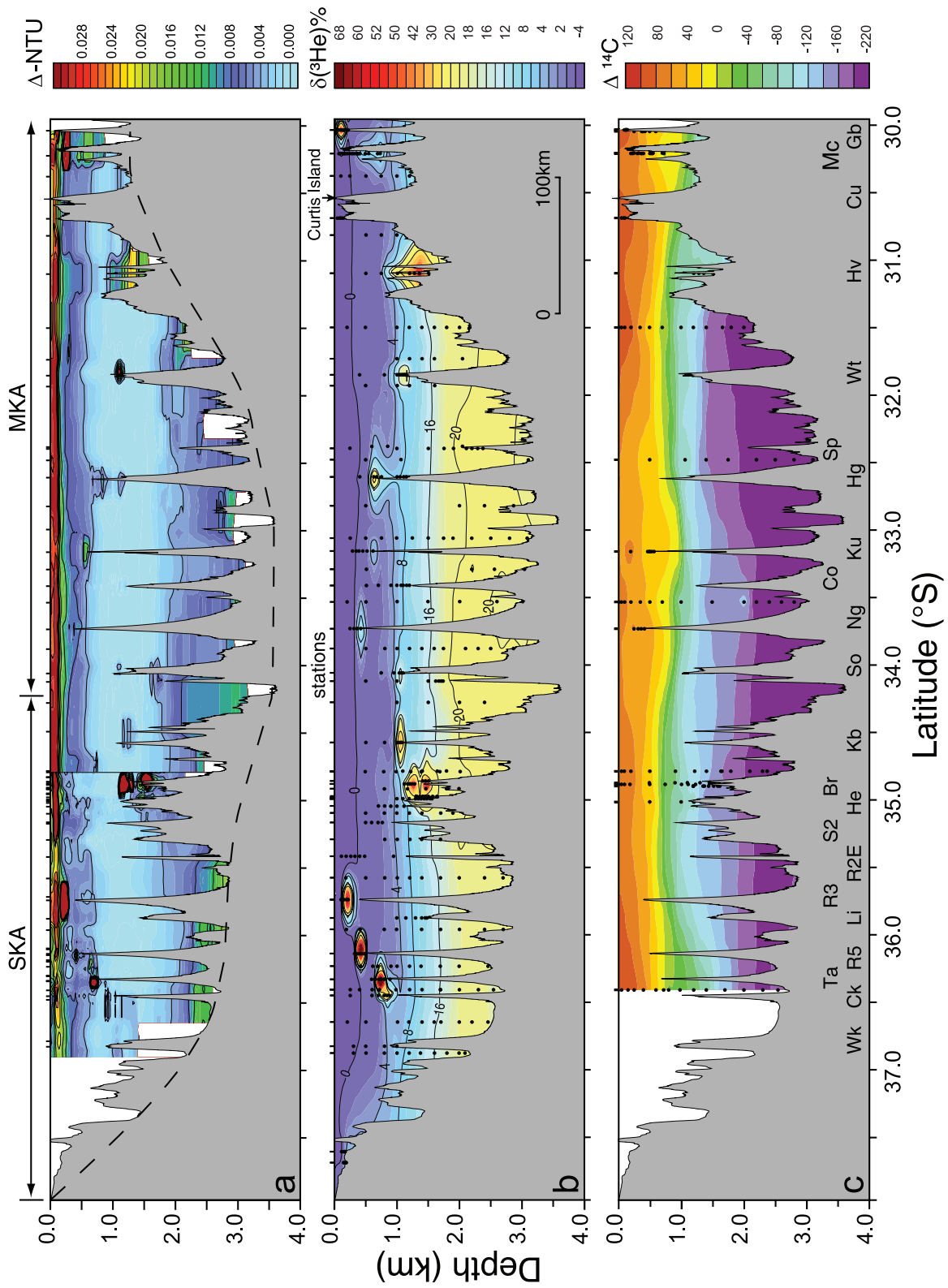


Figure 6

an abrupt increase (enrichment), and then a fairly uniform decrease down to $\sim 2,000$ m. Thereafter, $\delta^{13}\text{C}$ values are mostly constant to depths $>3,000$ m. This structure likely reflects the effects of biological activity in the water column rather than being directly related to hydrothermal activity.

[31] The carbon yields of each water sample, expressed as mg C per kg of water with errors of $\pm 10\%$, are shown in Figure 5c. Although the yield at a given depth covers a range, individual casts show a relatively steady increase in carbon content with depth. For example, there is an apparent steady increase in carbon content to about 1,500 m with a change to uniform concentrations below this depth until around 2,500 m, whereupon carbon concentrations decrease slightly to depths $>3,000$ m. Two anomalously low points were seen at station T02A-13, near the rim of Healy caldera. See Appendix A, section A3 for further information on the data used to compile Figures 5 and 6c (see below), and the methods used to obtain those data.

3. Discussion

3.1. Mid-Kermadec Versus Southern Kermadec Arc Venting

[32] The incidence of venting for volcanic centers along MKA is 82% (9 of 11), or 83% if we include Raoul Island (Figure 6). This compares with 67% (8 of 12, now including Kibblewhite) for volcanic centers of the SKA [de Ronde *et al.*, 2001]. Cole and Speight were the only volcanic centers sur-

veyed during NZAPLUME II that had no obvious venting. For Speight at least, this may in part be due to its small constructional volume of 14 km^3 which was possibly not large enough to sustain prolonged hydrothermal activity and/or was not periodically replenished by magmatic events.

[33] Intensity of venting associated with the MKA centers (as defined by the thickness and areal extent of the plumes, together with the concentration of gases and metal species in those plumes) is, however, generally much more subdued than those of the SKA, especially in the southern part of the NZAPLUME II survey area. For example, the highest $\delta^3\text{He}$ value measured for a plume from the MKA is 65% (Giggenbach), with an average for all plumes of 29%. By comparison, $\delta^3\text{He}$ maxima for plumes from the SKA have values up to 116% [de Ronde *et al.*, 2001], with an average of 66% for all the plumes, or more than double that of the MKA volcanic centers. The Macauley and Giggenbach centers are the exception to subdued venting along the MKA, and so too Raoul Island, considering the largely hydrothermally driven eruption that occurred there on March 17, 2006 (<http://data.geonet.org.nz/geonews/2006/03/17-march-2006-raoul-island-volcano.html>). Raoul and Macauley are both dominated by calderas and represent the two largest volcanic centers along the MKA (Table 1), and together with Curtis, clearly sit atop the Kermadec Ridge. Thus, in contrast to small volcanic centers like Speight, those centers located in the northern section of the MKA are apparently underlain by much larger

Figure 6. Combined long axis plots for the southern Kermadec arc (SKA) and mid-Kermadec arc (MKA). (a) Light-scattering results. Relatively intense venting is more noticeable for plumes along the SKA, or above volcanoes located on the Kermadec Ridge in the northern part of the MKA. The vertical line north of Brothers volcano separates the NZAPLUME I survey (March 1999) from the NZAPLUME II survey (May 2002). Data from the two surveys were gridded and contoured separately; differences in the surface layer are due to the time separating the two surveys and seasonal influences. Long dashes depict depth to the seafloor. (b) The $\delta^3\text{He}$ results. Helium anomalies associated with hydrothermal venting are superimposed on background values for the ocean in this region. Again, plumes with the highest concentrations of $\delta^3\text{He}$ occur over SKA and northern MKA volcanic centers. A deep He plume is seen in the midpart of the section, between water depths of $\sim 2,000$ and $3,200$ m. (c) $\Delta^{14}\text{C}$ results. A steady decrease in $\Delta^{14}\text{C}$ values is shown with depth in the profile shown. The $\Delta^{14}\text{C} = -100\text{‰}$ contour can be taken as the approximate demarcation between bomb contaminated water and that having only natural radiocarbon [Key, 2001]. The densest Pacific water, known as Circumpolar Deep Water, has its origin in the Southern Ocean and flows northward along the seafloor. Along its pathway it ages, warms, and mixes with overlying water and slowly upwells, resulting in a water mass known as the Pacific Deep Water. This mass is then thought to flow southward, with the core of the flow centered around 2,500 m, represented in the figure by the low $\Delta^{14}\text{C}$ values below $\sim 2,200$ m [cf. Key, 2001, Figure 6]. The $\Delta^{14}\text{C} = -40\text{‰}$ contour at $\sim 1,000$ m depth shows an undulating pattern with a wavelength of ~ 300 km that may reflect the bottom topography. Superimposed on the general background are smaller “upwellings” of more negative values which are associated with hydrothermal activity and mixing inside caldera volcanoes, such as Brothers ($\sim 34.8^\circ\text{S}$). Note that the MKA also includes Raoul Island, which is not shown but which would plot to the north (right) of Giggenbach (Gb) volcano by ~ 115 km at the same scale. Abbreviations: Wk, Whakatane; Ck, Clark; Ta, Tangaroa; R5, Rumble V; Li, Lillie; R3, Rumble III; R2E, Rumble II East; S2, Silient II; He, Healy; Br, Brothers; others as given in the caption to Figure 4.



magma chambers, ensuring a steady supply of heat to drive the hydrothermal systems.

[34] The chemical composition of MKA plumes is consistent among most of the centers. Kibblewhite, Sonne, Ngatoroirangi, Kuiwai, Haungaroa, Wright and to a lesser degree Havre, all have modest values for $\delta^3\text{He}$, small shifts in ΔpH , no detectable H_2S , low concentrations of total dissolvable Fe and Mn, and low (and internally consistent) Fe/Mn values (Table 2). By contrast, only four of the eight vent sites along the SKA had ΔpH anomalies smaller than -0.10 , with the other four ranging between -0.22 and -0.35 [*de Ronde et al.*, 2001]. Carbon dioxide concentrations account for $\sim 70\%$ of the measured pH anomalies along the SKA [*Massoth et al.*, 2003], which is also considered to be the case for most of the MKA sites. Hydrogen sulfide was also mostly undetected in plumes over SKA vent fields, although it was associated with three of the SKA centers (Rumble III, Rumble V, and Brothers cone; see Figure 1) with concentrations extremely high (18,700 and 4,250 nM) at two of these sites [*de Ronde et al.*, 2001]. Total dissolvable Fe was >100 nM for Tangaroa, Rumble III, Healy and Brothers (up to 4,720 nM at the cone site), while six of nine Fe/Mn values for plumes of the SKA were >5.7 , ranging up to 18.2 for the Brothers cone site [*de Ronde et al.*, 2001; *Massoth et al.*, 2003]. Two volcanoes (i.e., the summit plume at Rumble V, and Rumble II West) had Fe/Mn values less than unity, as seen for Havre of the MKA.

[35] Macauley cone and Giggenbach are distinct, with significantly greater chemical signatures associated with their hydrothermal plumes. Giggenbach has the single highest $\delta^3\text{He}$ and CH_4 values for this section of the arc, although they are coupled with a relatively small shift in ΔpH , suggesting a gas-rich system that may not be dominated by CO_2 . However, dives made by the submersible *Pisces V* during the 2005 NZASRoF (New Zealand American Submarine Ring of Fire) cruise showed we were not over the main vent region (where phase-separated gases were being vigorously expelled) during the NZAPLUME II sampling, but rather over a diffuse vent area where fluids were not phase-separated and only slightly H_2S (and probably CO_2) enriched. By contrast, Macauley cone has a smaller value for $\delta^3\text{He}$ but an order-of-magnitude greater ΔpH shift and similarly high CH_4 , indicative of gas-rich discharge (Table 2) and possibly oxidation and hydrolysis reactions as a result of sulfur gases mixing with seawater [*de Ronde et al.*, 2005]. Of those plumes analyzed for

their particulates, Macauley cone has by far the highest concentration of various elements. For example, total particulate S for Macauley is more than $10\times$ higher than for Giggenbach particulates, and $100\times$ higher than any other MKA site (Table 2). Similarly, Macauley cone particulate Fe concentrations far exceed those from the other MKA volcanic centers. Comparison of Macauley cone particulate data with SKA plumes resampled during NZAPLUME II, supplemented by samples collected during the 2004 NZAPLUME III and 2005 NZASRoF cruises, shows that this site has the highest concentrations of total S, Fe, Al, Mn, K Ba and Zn of any plume along the Kermadec arc at the time of sampling, with only the Brothers NW caldera site having higher Cu (Figure 7). The very high values of particulate Al at Macauley likely indicate the presence of natroalunite ($\text{NaAl}_3(\text{OH})_6(\text{SO}_4)_2$) in the samples and, when combined with the large shift in ΔpH and the high percentage of native S, is indicative of very acid fluids being expelled from this site [*de Ronde et al.*, 2005]. This would also explain the high K and Ba values as a result of rock dissolution. However, the very high concentrations of particulate Fe, high total dissolvable Fe, and a Fe/Mn value of 8.6, in concert with the more extreme enrichments in pH and particulate S and Al, suggests a magmatic fluid input may also be occurring at this site [*de Ronde et al.*, 2001; *Massoth et al.*, 2003]. The Brothers cone site is the only other along the arc where a magmatic input has demonstrably added high concentrations of Fe to the hydrothermal fluids [*de Ronde et al.*, 2005].

[36] In summary, intensity of venting is more subdued and chemical compositions generally more homogeneous for MKA plumes than for those of the SKA. This is most notable where the active arc front occurs behind the Kermadec Ridge. Where the front intersects the ridge, the relative intensity of venting (using light scattering as a proxy) increases noticeably, as does the concentration of gases and ionic species. This is especially true of Macauley cone and Giggenbach, and to a lesser degree Havre (Figures 1 and 6; Table 2). Similarly, metal-rich particulates were only recovered from plumes above sites on, or near, the ridge (Figure 7).

3.2. Large-Scale Factors Affecting Venting Along the Mid-Kermadec Arc

[37] Mapping of Kermadec arc volcanic centers shows that the active arc front lies behind the

Kermadec Ridge (i.e., in the backarc) until Haungaroa, near 32°37'S (Figure 6). Thereafter, the arc front gradually shifts to the east where it eventually intersects the ridge, with the volcanic centers initially located on the western flank of the ridge, and in the case of Wright, Curtis, Macauley and Raoul at the northern end of the survey, right on top of the ridge (Figure 1). A profile along the Kermadec arc from Whakatane to Giggenbach confirms that the seafloor shoals north of Haungaroa toward Giggenbach, but that it also shoals south of Sonne toward Whatakane (Figure 6). These changes in depth coincide with changes in the average spacing between the volcanic centers. That is, there is a statistically significant change from south to north in the average spacing of volcanic centers, increasing from 30 km in the back-arc of the SKA section, to 45 km in the back-arc of the MKA arc section, and finally to 58 km on the Kermadec Ridge. In addition, at both ends of the profile shown in Figure 6 where the seafloor shallows, hydrothermal plumes are much more intense (although not less frequent) than along the deepest part of the section, between Sonne and Haungaroa. We next consider several factors that may influence the location of volcanic centers and the intensity of their hydrothermal activity.

[38] The melting of mantle at convergent plate boundaries is considered to be controlled mainly by two mechanisms: (1) fluxing of fluids released from the subducted slab into the overlying mantle wedge [e.g., *Tatsumi*, 1989] and (2) disturbance of the mantle by the descending plate inducing convection in the mantle wedge, causing the ascent of hotter mantle material from depth [e.g., *Kincaid and Sacks*, 1997; *Schmidt and Poli*, 1998]. Both these mechanisms are typically portrayed as two-dimensional cross-sectional models of the convergent boundary. However, more recently the third dimension, along-strike length, has been considered important in understanding magma production along these boundaries. For example, Quaternary volcanoes in the northeast of Japan have been shown to be grouped into volcanic “clusters” (centers in this paper) that have an average width of 50 km and are separated by gaps of 30–75 km [*Tamura et al.*, 2002], remarkably similar to the spacings recorded for the MKA (Table 1). These authors suggest that a minimum spacing of 30 km is needed to define discrete volcanic centers; the shortest distance reported between centers of the MKA is 31 km. The Japanese volcanic centers have been interpreted as being related to locally

developed hot regions within the overlying mantle wedge that take the form of inclined, 50-km-wide fingers, each of which extends from >150 km below the back-arc region toward the shallower (~50 km) mantle region beneath the volcanic front [*Tamura et al.*, 2002]. The volcanoes are then built immediately above the tips of these “hot mantle fingers.” The fingers are associated with low-velocity regions in the mantle wedge, with negative Bouguer (gravity) anomalies thought to represent magma supplied from those fingers [*Tamura et al.*, 2002]. Conversely, the gaps between volcanic centers are not host to any mantle fingers and are relatively high-velocity zones.

[39] This model appears applicable to our observations of the SKA and MKA volcanoes. However, it does not explain the increased thickness of the crust in the SKA arc region, nor why volcanoes in this region and those in the northern-most part of the MKA are considerably more hydrothermally active than those where the seafloor is deepest, and the crust thinner. Recent seismic tomography studies show similar low-velocity zones underlie volcanically active regions of the central North Island of New Zealand that are located in the mantle wedge west of the plate margin [*Reyners et al.*, 2006]. These zones are also spaced along the strike of the subduction zone and are interpreted as significant volumes of partial melts in the mantle wedge, produced by dehydration of the subducting slab. The lowest velocity zones are located about 30 km from the upper surface of the mantle wedge. In addition, another low-velocity zone was identified beneath the central North Island which coincides with the upper plane of the dipping seismic zone, extending to a depth of ~65 km, which *Reyners et al.* [2006] ascribe to subduction of the 17-km-thick Hikurangi Plateau (Figure 8).

[40] On the basis of crustal thickness, bathymetric depth, and petrologic studies [*Mortimer and Parkinson*, 1996, and references therein], the Hikurangi Plateau has been classified as a large (350,000 km²), Early Cretaceous oceanic plateau of mainly basaltic composition. Today it abuts, and is being subducted beneath, the North Island of New Zealand. The margin of the northern-most corner of the Hikurangi plateau is identified by inflection of the ~5,000 m bathymetric contour off the NE coast of East Cape where it strikes subparallel to the Kermadec Trench (Figure 8). If we then project the plateau margin (Rapuhia Scarp) toward the NW where it would intersect the Kermadec arc, we see that it does so near the Kibblewhite volca-

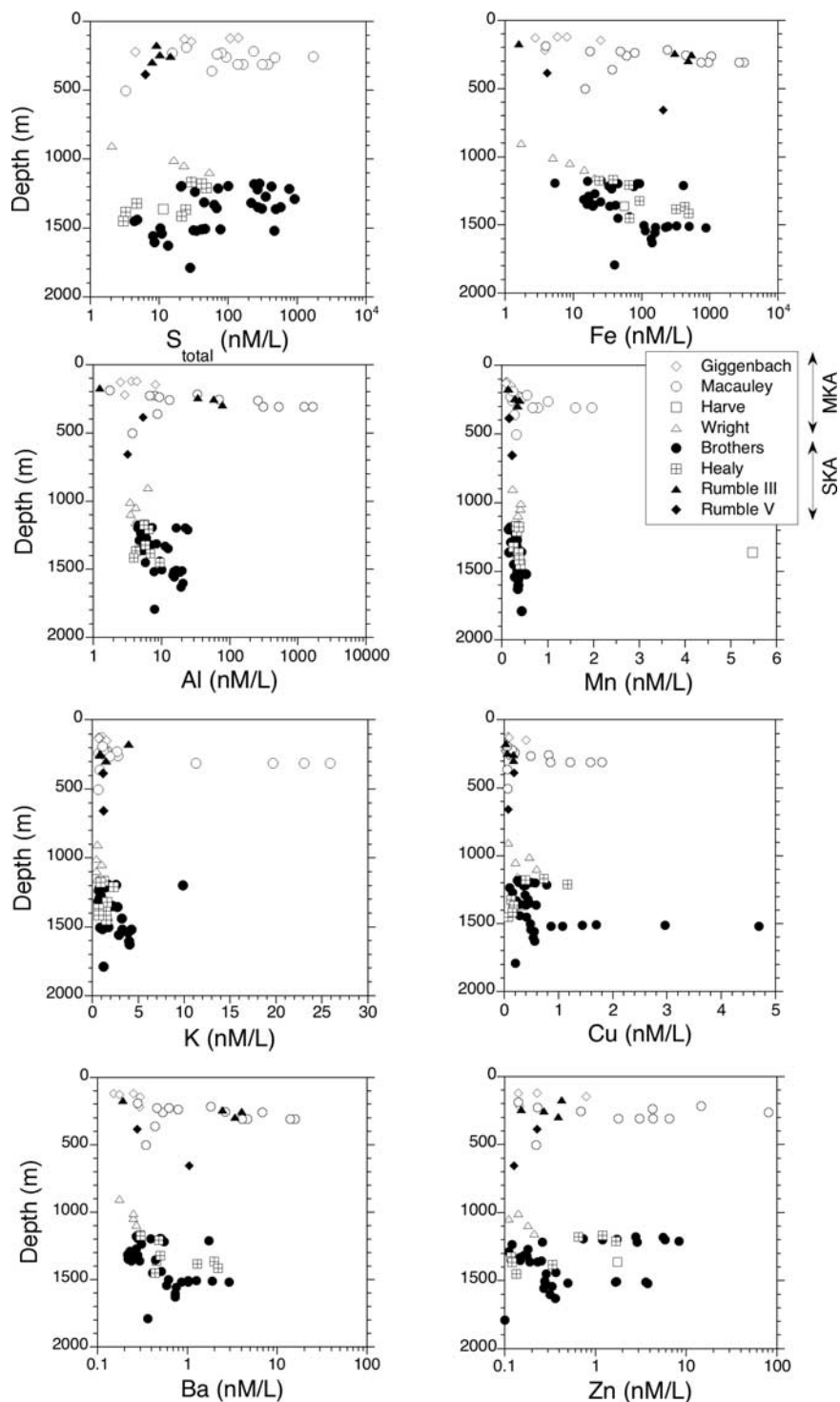


Figure 7. Plots of particulate data for Kermadec arc hydrothermal plumes. Data shown here are for both MKA and SKA volcanic centers largely collected during the 2002 NZAPLUME II cruise, although supplemented by samples collected during the 2004 NZAPLUME III and 2005 NZSRoF cruises. Macauley cone is the only volcano of the MKA that shows the high concentrations of the metals Fe, Cu, and Zn, together with Ba, that are seen in sites like Brothers and Healy of the SKA. Acidic vent fluids and high degrees of water/rock interaction at Macauley are given by high concentrations of Al, total S, and K.

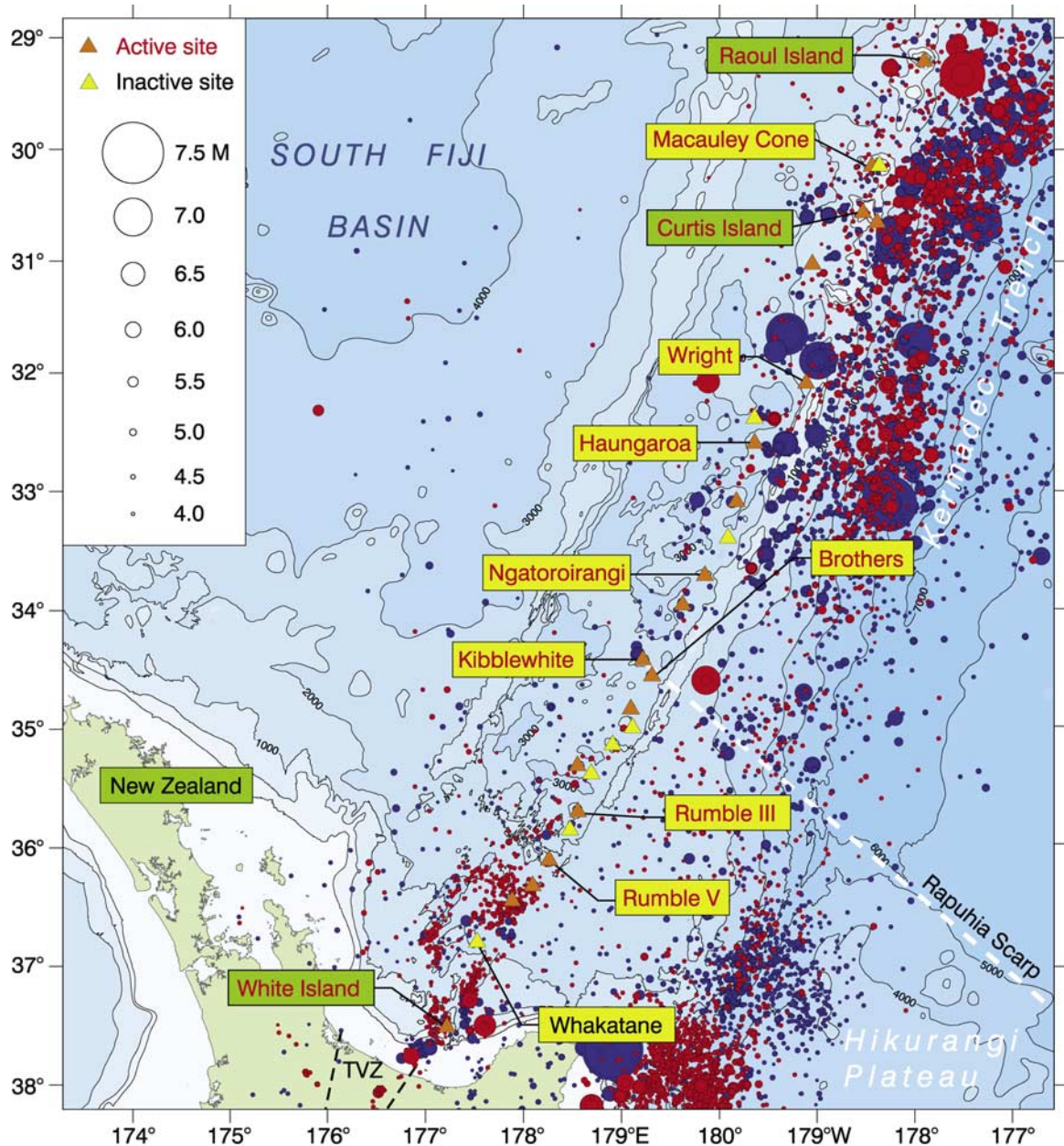


Figure 8. Earthquake epicenters from the IRIS Data Management Center for the Kermadec arc region, for the period January 1990 through June 2006. Red circles are for earthquakes shallower than 13 km; blue circles are for earthquakes deeper than 13 km but shallower than 60 km. Earthquakes deeper than 60 km are not shown. The size of the circle is proportional to the earthquake magnitude (see legend). Also shown for reference are select locations of volcanic centers and the margin of the Hikurangi Plateau, as given by the Rapuhia Scarp. There is a notable decrease in density of earthquake epicenters both along the arc and in the trench south of where the Hikurangi Plateau is thought to intersect the Kermadec arc, near the Kibblewhite volcanic center (dashed white line).

nic center. This is coincident with an abrupt change in depth to the seafloor immediately north of this center. Moreover, if we assume that volatiles fluxing from a subducting slab will be a given amount for a given thickness of slab, then subduction of the Hikurangi Plateau (which is at least twice as thick

as normal oceanic lithosphere and which includes up to 2 km of sediment [Davy and Wood, 1994; B. W. Davy, personal communication, 2006]) means we could expect at least twice as many fluids to be released from the crust of the down-going slab. This would in turn mean significantly more partial

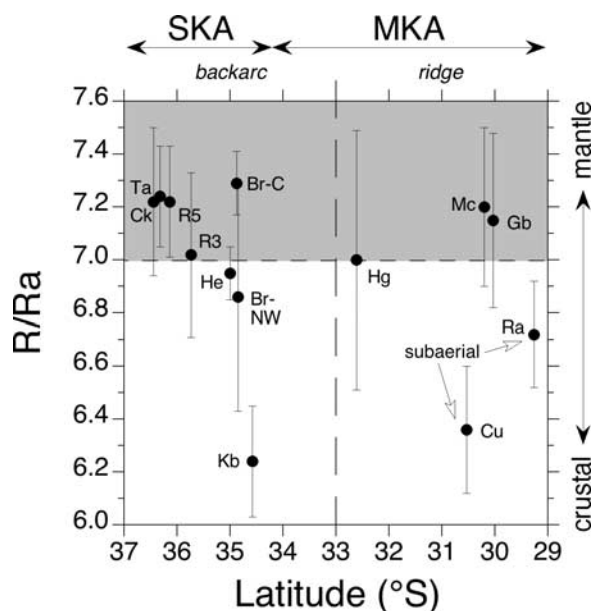


Figure 9. R/Ra plot (where $R = {}^3\text{He}/{}^4\text{He}_{\text{sample}}$ and $R_a = ({}^3\text{He}/{}^4\text{He})_{\text{air}}$) for hydrothermal plumes from SKA and MKA volcanic centers and, for comparison, fumarolic discharges from geothermal systems on Curtis and Raoul islands. Plume R/Ra values were extrapolated from samples which contained sufficient concentrations of helium. The value for Macauley is from vent fluids as extrapolation from the plume data was inconclusive. Comparison between extrapolated plume R/Ra values and values obtained from vent fluids for the same site show results coincide within ≤ 0.2 . For example, vent fluids collected during the 2004 *Shinkai 6500* dives on the Brothers NW caldera site have an average R/Ra value of 6.93, very similar to the 6.86 value derived from the plume data, only with a smaller error (± 0.2 versus ± 0.43). The most hydrothermally active sites of the SKA and northern MKA have the most nonradiogenic (mantle) R/Ra values. Most of the volcanoes plotting in the area shaded in gray have abundant evidence for magmatic volatiles contained in their hydrothermal plumes [de Ronde et al., 2001, 2005] (Table 2) Abbreviations: Br-NW, Brothers NW caldera; Br-C; Brothers cone; Cu, Curtis Island; Ra, Raoul Island; others as given in the captions to Figures 4 and 6.

melting would occur in the overlying mantle wedge, and so providing a greater supply of magma, effectively thickening the crust in this region by underplating. A greater magma supply would ensure that hydrothermal systems associated with the resultant volcanoes would be sustained for longer periods. Thus the addition of the Hikurangi Plateau during subduction of the Pacific plate beneath the Australian plate could explain both the change in depth of the seafloor and current intensity of hydrothermal venting of the volcanoes south of Kibblewhite. This is consistent with

currently available seismicity data which shows far fewer earthquakes south of the projected intersection of the Hikurangi Plateau with the Kermadec arc (Figure 8), a feature commonly associated with the subduction of oceanic plateaux [e.g., Vogt et al., 1976]. As subduction of the Hikurangi Plateau has been sweeping southward at 4 cm yr^{-1} , the greater-than-normal magma supply has effectively been “switched off” for the Kibblewhite, Sonne, Ngatoroirangi, Cole and Kuiwai volcanic centers, in some cases for a considerable period of time. Hence these hydrothermal systems today are much more subdued, or extinct.

[41] Subduction of the Hikurangi Plateau, however, does not explain the thick crust and the intensity of venting north of Haungaroa, and especially from Havre northward (Figure 6). These volcanic centers progressively merge with the Kermadec Ridge until Curtis where they mark the ridge itself (Figure 1). Here, they are typically large and are dominated by caldera complexes that are, on average, double the size of SKA calderas and half as large again as MKA cone complexes (Table 1). The Kermadec Ridge is older, thicker, and hence colder than the volcanic centers that comprise the arc front. The thick crust inferred in the northern part of the MKA (Figure 6), given by the shallowing depth of the seafloor, is thus mostly older than the Kermadec Ridge that has the arc front superimposed upon it. The change in crustal thickness of the overlying plate is a result of the original Tonga Platform being eroded between 31°S and $35\text{--}36^\circ\text{S}$ in the wake of oblique subduction of the Hikurangi Plateau [Collot and Davy, 1998; Davy and Collot, 2000].

[42] Recent tomographic results in Japan and New Zealand suggest that the location of volcanoes may also be controlled by where the corner flow in the mantle wedge meets the base of the crust [Hasegawa and Nakajima, 2004; Reyners et al., 2006]. A corollary to this is that crustal thickness in the overlying plate should play an important role on volcano location and spacing. One approach to volcano spacing is to treat it as a Rayleigh-Taylor instability, i.e., diapirism of more buoyant magma through denser crust. In this case the disturbance with the shortest time constant grows and dominates the instability, and in a simple two-layer case the wavelength of the instability is $\sim 2.6 \times$ layer thickness [Turcotte and Schubert, 2002]. For a volcanic center spacing of 45 km in the backarc of the MKA this suggests a crustal thickness of ~ 17.5 km. For a spacing of 58 km where the arc front merges with the Kermadec Ridge in the MKA

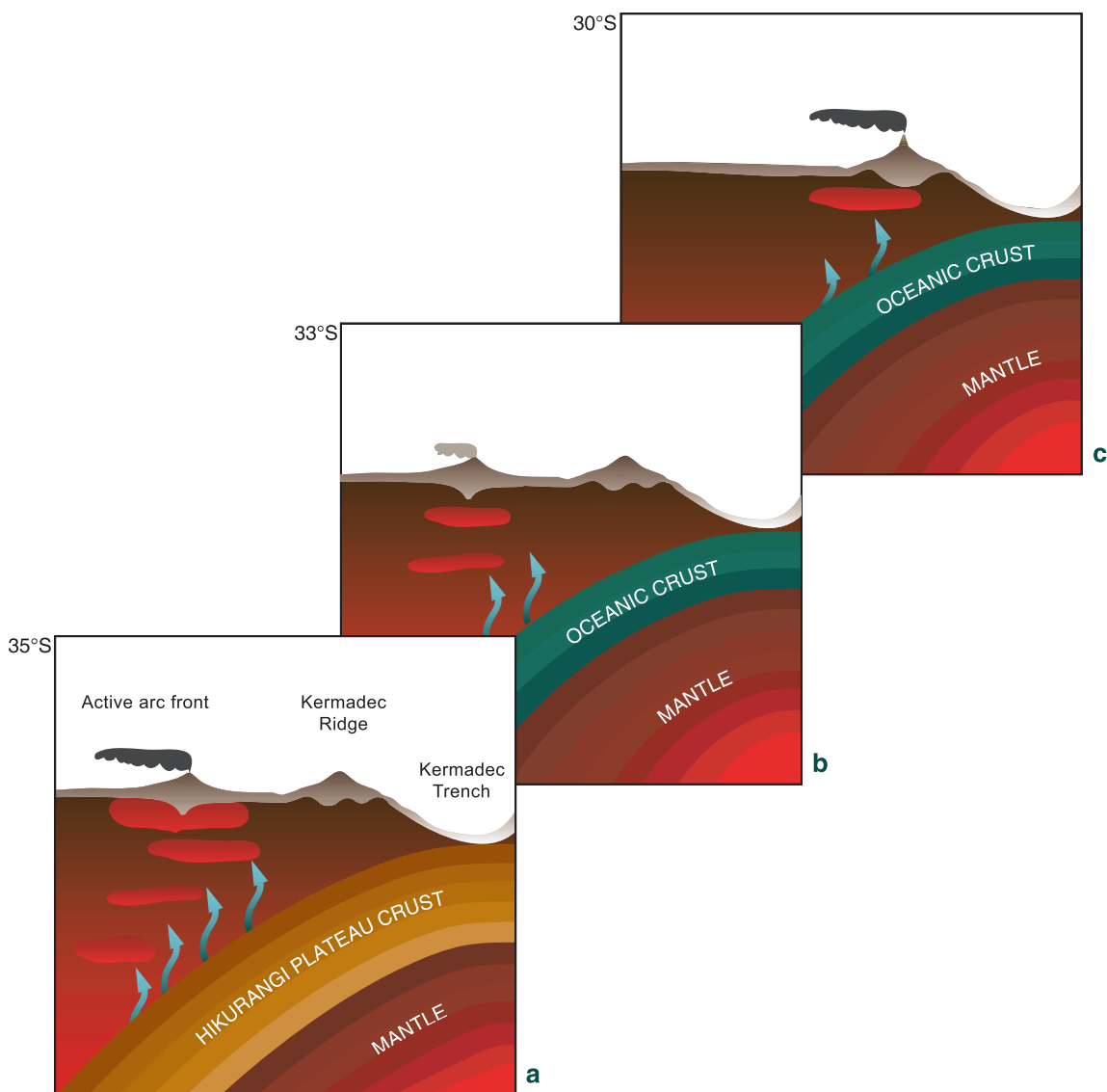


Figure 10. Cartoon model of subduction along the SKA and MKA showing the effect of the subducting Hikurangi Plateau on magma supply to volcanic centers located in the Kermadec backarc and along the Kermadec Ridge. (a) Example of section through the SKA south of 34.5°S. Here, the shallower dipping 17-km-thick Hikurangi Plateau crust on the Pacific Plate is being subducted beneath the Australian Plate to the west. The increased thickness of the Hikurangi Plateau crust means more water per strike km is being driven off the subducting slab, resulting in greater degrees of partial melting and hence a larger supply of magma to drive the hydrothermal systems of the active arc front. (b) Section through the southern portion of the MKA at 33°S. Here, there is no present-day subduction of the Hikurangi Plateau, so smaller supplies of magma are available to sustain the hydrothermal systems. The southward migration of the Hikurangi Plateau margin will have produced a thinner Kermadec Ridge as the crust collapsed, or “erosion” occurred, behind the retreating margin. (c) Representative section through the northern portion of the MKA at 30°S where there has been no subduction of the Hikurangi Plateau. Here, “normal” subduction of the Pacific Plate prevails, only the crust will be thicker with no associated collapse, as shown by the bulging keel beneath the Kermadec Ridge. As a consequence, magmas will pond beneath the crust and make fewer, but larger, chambers that will also show more evidence for crustal assimilation. Figure not to scale.

we calculate a crustal thickness of ~ 22.5 km. These values are consistent with refraction measurements made by *Shor et al.* [1971] of crustal thickness on the Kermadec Ridge, from 16 km at 34.2°S (near Kibblewhite) increasing to 19 km at 33.07°S (just north of Kuiu; see Figure 6). Our suggestion of Rayleigh-Taylor instability to explain volcanic center spacing has been suggested by others for the mantle [e.g., *Marsh and Carmichael*, 1974]. Nevertheless, our suggestion that it occurs in the crust is not inconsistent with the hot finger model of *Tamura et al.* [2002], as once magma conduits are established through the crust it is likely that mantle flow will become organized to feed these conduits.

[43] Larger magma bodies would also mean longer residence in the crust which in turn would induce more evolved (high silica) compositions, forming the dacite calderas seen along the ridge [cf. *Smith et al.*, 2003; *Wright et al.*, 2006]. Calderas commonly host very active hydrothermal systems and when combined with a sustained heat source, might explain why venting is also so intense along the northern section of the MKA (Figure 6). Three of the four volcanic centers with the highest $\delta^3\text{He}$ maxima along the MKA (i.e., Hangaroa, Havre and Giggenbach) sit on the Kermadec Ridge (Table 2) suggesting a greater supply of primordial He to these centers. Plotting available R/Ra values for all the Kermadec volcanic centers shows that helium with a more magmatic/mantle (or less radiogenic) component is found associated with most of the submarine volcanic centers, and especially those with evidence for magmatic volatiles being expelled by the vents. Only the three volcanic centers at the northern end of the SKA, i.e., Healy, the old NW caldera system at Brothers, and especially Kibblewhite, together with the subaerial geothermal systems on Curtis and Raoul islands, have more radiogenic, or crustal helium input into their hydrothermal systems (Figure 9).

[44] In summary, the only part of the margin which is “normal” is the northern part of the MKA after the arc front has intersected the Kermadec Ridge. The Hikurangi Plateau has then modified the remainder of the section shown in Figure 6 through tectonic erosion in the southern part of the MKA as it migrated southward, and through an increased volume of fluid to flux melt in the SKA today (Figure 10). Both these effects have influenced the longevity of the associated hydrothermal systems. Systems that have operated for several thousands of years may have experienced the necessary con-

ditions to form large polymetallic mineral deposits. It is therefore conceivable that those hydrothermal systems of the MKA, including those experiencing a period of quiescence, could in fact be host to large mineral deposits, particularly if we consider the source for sustained magma generation (i.e., the subduction of the Hikurangi Plateau) was likely once beneath these volcanic centers in the recent past [*Davy and Collot*, 2000].

Appendix A: Methods

A1. Helium Isotope Measurements (See Table A1)

[45] Upon recovery of the CTDO-rosette package, samples for helium analysis were immediately sealed into copper tubing using a hydraulic crimping device [*Young and Lupton*, 1983]. The samples were returned to the laboratory and processed on a high-vacuum extraction line that separates the dissolved gases from the water. At the end of this process, the extracted gases are sealed into a glass ampoule constructed of alumino-silicate glass (Corning type 1720 or 1724), which has low helium permeability. Helium concentrations and helium isotope ratios were then determined using a 21-cm radius, dual-collector mass spectrometer specifically designed for helium isotope measurements. The 1σ precision for the $^3\text{He}/^4\text{He}$ ratio determinations is about 0.2% in $\delta^3\text{He}$, where $\delta^3\text{He}(\%)$ is the % increase in the $^3\text{He}/^4\text{He}$ ratio above the atmospheric ratio. Thus $\delta^3\text{He} = 100 [(^3\text{He}/^4\text{He})_{\text{Sample}} / (^3\text{He}/^4\text{He})_{\text{Air}} - 1]$ where $(^3\text{He}/^4\text{He})_{\text{Air}} = 1.39 \times 10^{-6}$. The 1σ precision for the absolute ^3He and ^4He concentrations is about $\pm 1\%$. Table A1 includes all those data used to compile Figure 4b. It also includes data for some volcanoes from the SKA, resampled during the NZAPLUME II cruise, and used to supplement data collected during the 1999 NZAPLUME I cruise [*de Ronde et al.*, 2001], enabling some gaps in the profile to be in-filled (see Figure 6b).

A2. Particulate X-Ray Fluorescence Analysis (See Table A2)

[46] Particulate matter samples were collected passing plume waters through 37 mm diameter, 0.4 μm pore size polycarbonate filters (Nucleopore). The filters were dried, weighed, and analyzed by X-ray primary- and secondary-emission spectrometry with a Rh source and Mo, Ti, Se, and Co secondary targets using a nondestructive thin-



Table A1 (Representative Sample). Helium Isotope Data for Mid-Kermadec Arc Seawater Samples^a [The full Table A1 is available in the HTML version of this article at <http://www.g-cubed.org>]

Volcano Location	Cast/Bottle Number	Depth, km	³ He, ccSTP/g	⁴ He, ccSTP/g	δ(³ He)%
Yokosuka 34° 42.37'S/ 178° 34.27'E	V02A01 B9A	0.248	5.42E-14	3.93E-08	-0.7
	V02A01 B6A	0.752	5.63E-14	3.99E-08	1.5
	V02A01 B4A	0.998	5.86E-14	4.04E-08	4.3
	V02A01 B3A	1.040	6.01E-14	4.05E-08	6.7
	V02A01 B1A	1.079	6.27E-14	4.16E-08	8.4
Rapuhia 34° 46.74'S/ 178° 30.32'E	V02A02 B8A	0.010	5.29E-14	3.87E-08	-1.6
	V02A02 B6A	0.400	5.40E-14	3.90E-08	-0.2
	V02A02 B4A	0.598	5.55E-14	3.95E-08	1.0
	V02A02 B3A	0.648	5.58E-14	3.97E-08	1.1
	V02A02 B2A	0.671	5.89E-14	4.11E-08	3.2
Giljanas 34° 46.57'S/ 178° 34.89'E	V02A02 B1A	0.677	5.89E-14	4.14E-08	2.5
	V02A03 B7A	0.199	5.38E-14	3.90E-08	-0.7
	V02A03 B6A	0.400	5.44E-14	3.92E-08	-0.1
	V02A03 B4A	0.602	5.58E-14	3.97E-08	1.0
	V02A03 B3A	0.650	5.64E-14	4.00E-08	1.6
Brothers- NW caldera 34° 52.29'S/ 179° 03.35'E	V02A03 B2B	0.686	5.68E-14	4.02E-08	1.6
	V02A03 B1A	0.710	5.69E-14	4.01E-08	2.1
	V02A04 B11A	0.494	5.50E-14	3.91E-08	1.1
	V02A04 B10A	0.903	5.75E-14	4.00E-08	3.4
	V02A04 B9A	1.100	6.16E-14	4.05E-08	9.4
Brothers-cone 34° 53.01'S/ 179° 04.04'E	V02A04 B17A	1.301	6.26E-14	4.09E-08	10.1
	V02A04 B7A	1.450	7.10E-14	4.17E-08	22.4
	V02A04 B6A	1.501	7.44E-14	4.23E-08	26.4
	V02A04 B4A	1.518	8.19E-14	4.31E-08	36.6
	V02A04 B3A	1.541	7.88E-14	4.30E-08	31.9
In-between Brothers/Kbw 34° 47.17'S/ 179° 10.49'E	V02A04 B2A	1.602	7.86E-14	4.30E-08	31.5
	V02A04 B1A	1.698	7.76E-14	4.27E-08	30.8
	V02A05 B23A	0.185	5.40E-14	3.88E-08	0.1
	V02A05 B21A	0.500	5.50E-14	3.89E-08	1.6
	V02A05 B5A	0.746	5.71E-14	4.02E-08	2.1
Kibblewhite- satellite cone 34° 41.03'S/ 179° 17.74'E	V02A05 B25A	1.006	5.87E-14	4.03E-08	4.9
	V02A05 B24A	1.112	6.20E-14	4.08E-08	9.3
	V02A05 B20A	1.171	6.31E-14	4.12E-08	10.2
	V02A05 B1A	1.230	6.39E-14	4.10E-08	12.0
	V02A06 B17A	1.093	5.99E-14	4.04E-08	6.7
Kibblewhite 34° 34.51'S/ 179° 15.30'E	V02A06 B23A	1.404	6.25E-14	4.11E-08	9.4
	V02A06 B5A	1.650	6.82E-14	4.19E-08	17.1
	V02A06 B25A	1.792	6.94E-14	4.20E-08	18.8
	V02A07 B17A	0.250	5.40E-14	3.89E-08	-0.2
	V02A07 B26A	0.998	5.76E-14	3.98E-08	4.1
Kibblewhite- satellite cone 34° 29.30'S/ 179° 14.13'E	V02A07 B23A	1.303	6.19E-14	4.08E-08	9.1
	V02A07 B21A	1.431	6.47E-14	4.12E-08	13.0
	V02A07 B25A	1.509	6.49E-14	4.09E-08	14.0
	V02A07 B24A	1.539	6.64E-14	4.17E-08	14.7
	V02A07 B20A	1.601	6.71E-14	4.19E-08	15.2
Kibblewhite 34° 29.30'S/ 179° 14.13'E	V02A07 B1A	1.635	6.74E-14	4.18E-08	16.0
	V02A08 B23A	0.501	5.53E-14	3.94E-08	1.0
	V02A08 B21A	0.804	5.62E-14	3.96E-08	2.3
	V02A08 B25A	1.001	5.85E-14	4.00E-08	5.1
	V02A08 B24A	1.025	6.77E-14	4.11E-08	18.5
Kibblewhite- satellite cone 34° 29.30'S/ 179° 14.13'E	V02A08 B20A	1.060	8.88E-14	4.35E-08	46.8
	V02A08 B8A	1.085	8.00E-14	4.26E-08	35.1
	V02A09 B23A	0.492	5.58E-14	3.97E-08	1.0
	V02A09 B15A	0.750	5.62E-14	3.96E-08	2.2
	V02A09 B21A	1.000	5.91E-14	4.02E-08	5.7
	V02A09 B5A	1.140	6.03E-14	4.06E-08	6.8

^aNotes: V, vertical cast; T, tow (yo); 02A, year and number of cruise (NZAPLUME II); 52, cast number; B19A, bottle number. Yokosuka, Rapuhia and Giljanas are not shown in Figure 4 or 6 as they occur ~106 km behind the Kermadec Ridge (see text). Latitude/longitude is given for position of vertical casts and at start of tow-yos.



Table A2 (Representative Sample). Particulate Analysis^a [The full Table A2 is available in the HTML version of this article at <http://www.g-cubed.org>]

Sample	Filter Number	Depth, m	Vol, L	Na, nM	Mg, nM	Al, nM	Si, nM	P, nM	S _{total} , nM	VS, nM
V02A04-2	GD15	1602	7.5	52.5	18.6	20.7	64.7	44.8	8	-8
V02A04-3	GD16	1541	7.9	106.2	18.9	14.7	49.7	39.3	11	-3
V02A04-4	GD17	1518	7.3	63.5	27.6	15.2	69.7	74.2	35	-4
V02A04-6	GD18	1501	7.2	31.7	13.2	10.1	41.3	36.5	10	-3
V02A04-7	GD19	1450	8	49.8	8.2	5.8	23.9	15.2	4	-2
T02A10-25	GD35	1438	5.15	68.1	11.3	9.4	39.5	21.8	5	-6
T02A10-27	GD36	1355	7.75	74.8	8.4	5.1	21.7	13.0	68	-11
T02A10-15	GD37	1350	6.35	17.5	4.2	6.2	23.4	8.2	575	458
T02A10-18	GD38	1519	7.45	63.0	65.4	18.6	138.7	255.0	466	149
T02A10-24	GD39	1193	5.45	23.9	3.2	7.2	28.0	1.5	100	-15
T02A12-2	GD40	1318	7.75	17.8	3.0	7.1	24.4	5.8	216	104
T02A12-28	GD41	1362	7.75	16.0	4.8	5.4	19.7	12.4	488	381
T02A12-4	GD42	1629	8.25	53.0	17.6	19.4	67.5	44.9	13	-2
T02A12-21	GD43	1557	8.85	23.3	18.3	15.3	59.7	49.8	8	-2
T02A42-21	GD20	218	8.2	91.8	6.6	2.9	18.6	2.5	4	-2
V02A42-8	GD26	120	7.7	42.5	4.7	3.6	37.1	6.9	139	73
V02A42-25	GD27	121	7.6	23.8	3.7	4.3	38.0	7.0	105	37
T02A03-25	GD24	145	5.3	64.8	6.8	8.2	44.4	8.8	29	-5
T02A03-4	GD25	128	9.45	21.4	3.3	2.5	30.7	3.4	23	-3
V02A24-23	GD21	1898	20.5	29.5	3.4	6.2	28.8	0.9	1	-1
V02A24-25	GD22	1898	20.5	37.4	3.1	5.5	25.5	0.8	1	-1
V02A37-13	GD23	1362	12.5	29.0	6.5	4.6	23.9	15.7	11	-2
V02A43-12	GD28	257	5.2	136.1	15.7	13.1	25.3	13.6	94	-7
V02A44-23	GD29	502	6.25	10.9	3.5	3.7	17.4	3.3	3	1
V02A44-28	GD30	361	7.65	15.6	5.3	8.7	17.8	10.2	58	-10
V02A44-7	GD31	227	7.05	152.3	12.2	8.0	15.2	11.9	79	-10
T02A06-3	GD32	255	7.05	54.7	32.7	69.7	44.4	64.4	1727	1347
V02A43-3	GD33	225	5.2	20.1	6.1	6.7	38.5	6.3	15	-9
T02A13-27	GD44	1208	7.95	73.3	12.6	6.6	27.6	23.6	49	-9
T02A13-20	GD45	1383	8.15	42.4	28.9	6.8	55.7	109.1	3	-8
T02A13-25	GD46	1451	7.75	13.2	7.0	9.5	43.1	19.4	3	-6
T02A14-4	GD47	1168	8.75	20.5	5.0	5.6	22.1	13.4	29	-7
T02A14-9	GD48	1322	9.75	41.6	13.4	5.8	29.5	32.6	5	-5
T02A15-13	GD49	295	7.25	55.0	42.9	77.7	30.6	65.3	8	-7
T02A16-3	GD50	170	8.45	124.4	8.9	1.2	7.6	1.5	9	-4
T02A17-8	GD51	240	8.25	30.9	24.9	33.8	24.4	37.1	10	-5
T02A17-2	GD52	252	7.65	39.4	35.1	58.0	27.6	56.5	15	-10
V02A48-27	GD53	385	6.5	17.6	2.9	5.3	22.2	2.0	6	-3
V02A49-49	GD54	655	5.95	56.4	18.7	3.2	22.4	49.8	1	-5

^aNotes: BDL, below detection limit; nM, nMol/L; S tot, total sulfur; VS, volatile sulfur; NVS, nonvolatile sulfur. Abbreviations: T, tow (yo); V, vertical east; O2A, year and number of cruise (NZAPLUME II); 44, cast number. For location of casts, see Table A1 and Figures 4 and 6.



Table A3 (Representative Sample). Carbon Isotope Data for Mid-Kermadec Arc Seawater Samples^a [The full Table A3 is available in the HTML version of this article at <http://www.g-cubed.org>]

Cast	Depth, m	$\delta^{13}\text{C}$, ^b ‰	$\Delta^{14}\text{C}$, ^c ‰	Carbon, ^d mg/kg	[¹⁴ C], ^e 10 ⁹ atoms/L	
T02A-03	118	0.75	93.2 ± 4.2	24.0	1.6	
	128	1.93	91.0 ± 4.2	24.2	1.6	
	144	1.72	84.5 ± 4.8	24.2	1.6	
T02A-06	233	1.02	88.5 ± 4.6	23.8	1.6	
	255	1.10	76.8 ± 4.4	23.9	1.6	
	326	1.01	61.8 ± 5.3	24.1	1.6	
	553	1.36	17.8 ± 5.5	24.3	1.5	
	700	1.36	4.2 ± 4.9	24.7	1.5	
	500	1.16	42.3 ± 4.0	25.3	1.6	
T02A-13	1000	0.78	-57.1 ± 3.9	23.9	1.4	
	1201	0.53	-84.1 ± 3.9	23.3	1.3	
	1208	0.89	-68.1 ± 3.8	26.1	1.5	
	1318	0.89	-134.0 ± 3.7	26.3	1.4	
	1323	0.84	-129.7 ± 3.3	26.8	1.4	
	1349	0.82	-144.5 ± 3.5	26.3	1.4	
	1383	0.81	-152.2 ± 3.6	26.6	1.4	
	1391	0.82	-140.3 ± 3.8	26.4	1.4	
	1451	0.71	-148.7 ± 3.6	26.3	1.4	
	1582	0.33	-150.7 ± 3.3	26.4	1.4	
	T02A-10	1193	1.00	-83.4 ± 3.7	26.1	1.5
		1193	0.99	-111.5 ± 3.5	26.2	1.4
		1194	1.03	-115.6 ± 3.7	26.1	1.4
1350		0.81	-138.0 ± 3.5	26.1	1.4	
1372		0.08	-141.0 ± 3.5	26.3	1.4	
1438		0.75	-153.1 ± 3.5	26.6	1.4	
1519		0.73	-163.5 ± 3.5	26.8	1.4	
1583		0.34	-124.8 ± 3.5	27.0	1.5	
1616		0.72	-161.6 ± 4.2	26.8	1.4	
1798		0.22	-158.2 ± 3.4	26.8	1.4	
1859		0.62	-162.3 ± 3.5	26.8	1.4	
V02A-04		494	1.20	33.4 ± 4.0	24.7	1.6
		903	1.14	-54.9 ± 3.8	25.2	1.5
	1100	0.96	-87.1 ± 3.9	25.4	1.4	
	1301	0.44	-112.7 ± 3.6	25.6	1.4	
	1450	0.69	-147.8 ± 3.8	25.9	1.4	
	1501	0.62	-149.1 ± 3.5	26.2	1.4	
	1518	0.57	-153.0 ± 3.5	26.2	1.4	
	1541	0.61	-155.2 ± 3.5	26.1	1.4	
	1602	0.55	-155.3 ± 3.5	26.0	1.4	
	1698	0.12	-158.1 ± 3.5	26.0	1.4	
	V02A-05	10	0.93	81.4 ± 4.1	24.1	1.6
		50	1.42	74.4 ± 4.0	24.2	1.6
		98	1.10	71.7 ± 4.0	24.7	1.6
185		1.06	66.7 ± 4.4	25.4	1.7	
500		1.19	17.1 ± 4.0	25.4	1.6	
746		1.25	-39.1 ± 3.6	25.8	1.5	
1006		1.08	-84.6 ± 3.7	25.9	1.5	
1112		0.44	-103.4 ± 3.4	26.0	1.4	
1230		0.93	-121.8 ± 3.5	26.2	1.4	
V02A-06	50	1.5	78.3 ± 4.4	24.1	1.6	
	95	1.1	75.0 ± 4.5	24.9	1.7	
	200	1.8	64.4 ± 4.3	24.8	1.6	
	501	1.4	20.3 ± 5.1	23.9	1.5	

^a Abbreviations: T, tow (yo); V, vertical cast; 02A, year and number of cruise (NZAPLUME II); 52, cast number. For location of casts, see Table A1 and Figure 4.

^b Stable isotope data have an uncertainty of ± 0.1‰.

^c Note that since $\Delta^{14}\text{C}$ refers to a difference from a standard, the quoted errors represent the fractional errors in the ¹⁴C measurements.

^d Precision of carbon concentration is estimated as better than ±0.3 mg/kg.

^e Precision of ¹⁴C concentration is estimated as ± 0.1 × 10⁹ atoms/L.



film technique [Feely *et al.*, 1991]. Total Particulate Sulfur (TPS) is the amount of sulfur determined under an atmosphere of nitrogen, nonvolatile sulfur (NVS) is the amount of sulfur determined in vacuo, and volatile sulfur (VS) is the difference between TPS and NVS [Feely *et al.*, 1999]. Nonvolatile sulfur is the sum of sulfur bound by sulfide and sulfate phases while volatile sulfur is thought to be elemental sulfur. The average precision for particulate Fe (PFe) and NVS was 2%, while TPS, VS, and particulate Cu (PCu) average 11%, 11% and 7%, respectively (see Table 2 and Figure 7).

A3. Radiocarbon (See Table A3)

A3.1. Sample Processing

[47] At each station water was collected in Niskin bottles over a depth range from surface to near the seafloor, or where there were indications that water from hydrothermal plumes was present. The water was stored in 250 ml glass bottles containing approximately 3 mg of mercuric chloride to suppress bacterial activity. The bottles were completely filled as soon as the water was brought to the surface, and tightly sealed with no headspace.

[48] At the Rafter Laboratory the inorganic carbon was extracted by transferring 110 ml of water to a flask. After the flask was sealed, 5 ml of phosphoric acid was added to the water and, after vigorous shaking, the flask was connected to a vacuum line and pumped. The acid had the effect of converting carbonate and bicarbonate ions to dissolved CO₂ which could be extracted from the water under vacuum. Vapor from the flask passed through two dry-ice/alcohol traps to remove water vapor, and the carbon was collected as CO₂ in a liquid nitrogen trap.

A3.2. Total Inorganic Carbon Determination

[49] Quantitative extraction of the inorganic carbon in the water was achieved by weighing (to within 0.1 mg) the reaction flask while empty, and again after the water was added. After the second weighing the phosphoric acid was added into a short sidearm in the flask neck, so that it did not contact the water, and a magnetic stirring “flea” was placed in the flask. When the flask was sealed it was tipped to allow the acid to mix with the water and shaken vigorously for 30 seconds. It was then connected to the vacuum system and rested on the magnetic stirrer. The flask tap was opened while the stirrer rotated at maximum speed to ensure that

there was sufficient turbulence to allow the entire water volume to be exposed at the surface.

[50] Once the CO₂ had been collected in the liquid nitrogen trap it was transferred to a calibrated volume and allowed to come to room temperature. A pressure transducer then allowed the quantity of gas to be calculated, and since the weight of water was known, the weight of carbon per kg of sample was obtained (see Figure 5c).

[51] The total inorganic carbon determination is part of the laboratory quality control procedures, to ensure proper extraction of the sample CO₂. The extraction efficiency of this system is estimated to be greater than 96%.

A3.3. The ¹³C Measurements

[52] A small portion of the pure CO₂ was analyzed for stable carbon isotope ratio on a Europa Scientific[®] Geo 20/20 mass spectrometer. The ¹³C measurement is necessary in order to reduce the measured ¹⁴C isotopic ratio to a standard $\delta^{13}\text{C}$ value (by convention, -25‰). This eliminates chemical fractionation effects in the CO₂ which would shift the ¹⁴C results. The stable isotope measurements have uncertainties of $\pm 0.1\text{‰}$.

[53] The above two steps form part of the standard procedure for analyzing seawater samples for ¹⁴C. However, while the quantities they determine can be regarded as “by-products” of the ¹⁴C analysis, they can yield useful data about the composition of the sample material, and hence have been included in the data set for this paper (e.g., see Figure 5b).

A3.4. The ¹⁴C Measurements

[54] The bulk of the extracted gas was converted to graphite by means of catalytic reduction with hydrogen over an iron catalyst at 700°C. The ¹⁴C measurement was performed on the graphite, using the GNS Sciences accelerator mass spectrometry (AMS) facility at Gracefield, Lower Hutt.

[55] The radiocarbon concentrations are expressed as $\Delta^{14}\text{C}$, defined as the $^{14}\text{C}/\text{C}_{\text{total}}$ ratio relative to the Modern Radiocarbon Standard ($^{14}\text{C}/\text{C}_{\text{total}} = 1.176 \times 10^{-12}$) after the sample stable carbon isotope ratio has been corrected to -25‰ . The $\Delta^{14}\text{C}$ values are expressed in parts per mil (‰).

[56] For the actual measurements, samples were measured against the international radiocarbon standard NBS (NIST) oxalic acid SRM-4990. The measurement procedure consisted of loading the AMS ion source (National Electrostatics Cor-



poration[®] MC-SNICS) with up to 40 graphite samples, comprising approximately 1 oxalic acid standard for each 6 unknowns plus one each of a tuning and background sample, and measuring each sample for 30 minutes or until the target precision of $\pm 0.4\%$ was reached. The parameter measured for each sample was the ratio of ^{14}C counts per unit ^{13}C current recorded by the AMS data acquisition system.

[57] The uncertainties in the ^{14}C results are due principally to the statistical precision of the ^{14}C measurements. The uncertainty in the ^{13}C measurement is small by comparison. The reported errors also include an instrumental component that is determined from a series of measurements on nominally identical graphite made from the oxalic acid standard. This component is estimated conservatively to contribute less than 2‰ to the final error, and is combined in quadrature with the sample statistical error (see Figures 5a and 6c).

Acknowledgments

[58] Access to detailed bathymetric maps generated during the preceding TAN02/05 cruise meant we were able to accurately locate our plume surveys during NZAPLUME II. We thank the captain and crew of the R/V *Tangaroa* for ensuring we enjoyed a safe and productive expedition. Discussion with C. J. Wilson, I. J. Graham, and R. J. Arculus helped clarify some aspects of this study for the senior author. We acknowledge the helpful input during the NZAPLUME II cruise by K. Britten, P. Hill, and M. Walkington. We thank J. Vodanovich for aiding the senior author in creating several of the figures. Constructive reviews by W. Seyfried, Jr., J. Seewald, and W. Bach improved this contribution. This is PMEL contribution 2978.

References

- Baker, E. T., R. A. Feely, C. E. J. de Ronde, G. J. Massoth, and I. C. Wright (2003), Submarine hydrothermal venting on the southern Kermadec volcanic arc front (offshore New Zealand): Location and extent of particle plume signatures, in *Intra-oceanic Subduction Systems: Tectonic and Magmatic Processes*, edited by R. Larter and P. Leat, *Geol. Soc. London Spec. Publ.*, 219, 141–161.
- Collot, J.-Y., and B. Davy (1998), Forearc structures and tectonic regimes at the oblique subduction zone between the Hikurangi Plateau and the southern Kermadec margin, *J. Geophys. Res.*, 103, 623–650.
- Davy, B., and J.-Y. Collot (2000), The Rapuhia Scarp (northern Hikurangi Plateau)—Its nature and subduction effects on the Kermadec Trench, *Tectonophysics*, 328, 269–295.
- Davy, B., and R. Wood (1994), Gravity modeling of the Hikurangi Plateau, *Mar. Geol.*, 118, 139–151.
- de Ronde, C. E. J., E. T. Baker, G. J. Massoth, J. E. Lupton, I. C. Wright, R. A. Feely, and R. G. Greene (2001), Intra-oceanic subduction-related hydrothermal venting, Kermadec volcanic arc, New Zealand, *Earth Planet. Sci. Lett.*, 193, 359–369.
- de Ronde, C. E. J., G. J. Massoth, E. T. Baker, and J. E. Lupton (2003), Submarine hydrothermal venting related to volcanic arcs, in *Giggenbach Memorial Volume*, edited by S. F. Simmons and I. G. Graham, *Soc. Econ. Geol. Geochem. Soc. Spec. Publ.*, 10, 91–109.
- de Ronde, C. E. J., et al. (2005), Evolution of a submarine magmatic-hydrothermal system: Brothers volcano, southern Kermadec arc, New Zealand, *Econ. Geol.*, 100, 1097–1133.
- Embley, R. W., et al. (2006), Long-term eruptive activity at a submarine arc volcano, *Nature*, 441, 494–497.
- Faure, K., J. Greinert, I. A. Pecher, I. J. Graham, G. J. Massoth, C. E. J. de Ronde, I. C. Wright, E. T. Baker, and E. J. Olson (2006), Methane release at the top of the gas hydrate stability zone of the Hikurangi margin, New Zealand, *N. Z. J. Geol. Geophys.*, 49, 503–516.
- Feely, R. A., G. J. Massoth, and G. T. Lebon (1991), Sampling of marine particulate matter and analysis by X-ray fluorescence spectrometry, in *Marine Particles: Analysis and Characterization*, *Geophys. Monogr. Ser.*, vol. 63, edited by D. C. Hurd and D. W. Spencer, pp. 251–257, AGU, Washington, D. C.
- Feely, R. A., E. T. Baker, G. T. Lebon, J. F. Gendron, J. A. Resing, and J. P. Cowen (1999), Evidence for sulfur enrichment in hydrothermal particles at Axial Volcano following the January, 1998 eruption, *Geophys. Res. Lett.*, 26, 3649–3652.
- Gamble, J. A., and I. C. Wright (1995), The southern Havre Trough: Geological structure and magma petrogenesis of an active backarc rift complex, in *Backarc Basins: Tectonics and Magmatism*, edited by B. Taylor, pp. 29–62, Plenum, New York.
- Gavrilenko, G. M. (1984), Hydrochemical methods for the discovery and study of submarine volcanic activity (in Russian), *Volcanol. Seismol.*, 5, 40–48.
- Hasegawa, A., and J. Nakajima (2004), Geophysical constraints on slab subduction and arc magmatism, in *The State of the Planet: Frontiers and Challenges in Geophysics*, *Geophys. Monogr. Ser.*, vol. 150, edited by R. S. J. Sparks and C. J. Hawkesworth, pp. 81–94, AGU, Washington, D. C.
- Hulston, J. R., and J. E. Lupton (1996), Helium isotope studies of geothermal fields in the Taupo Volcanic Zone, New Zealand, *J. Volcanol. Geotherm. Res.*, 74, 297–321.
- Ishibashi, J., H. Wakita, K. Okamura, E. Nakayama, R. A. Feely, E. T. Baker, K. Marumo, and A. Maruyama (1997), Hydrothermal methane and manganese variation in the plume over the superfast-spreading southern East Pacific Rise, *Geochim. Cosmochim. Acta*, 61, 485–500.
- Key, R. M. (2001), Ocean process tracers: Radiocarbon, in *Encyclopedia of Ocean Sciences*, edited by J. Steele, S. Thorpe and K. Turekian, pp. 2338–2353, Elsevier, New York.
- Kincaid, C., and I. S. Sacks (1997), Thermal and dynamical evolution of the upper mantle in subduction zones, *J. Geophys. Res.*, 102, 12,295–12,315.
- Lupton, J. E. (1998), Hydrothermal helium plumes in the Pacific Ocean, *J. Geophys. Res.*, 103, 15,853–15,868.
- Lupton, J. E. (2001), Ocean process tracers: Volcanic helium, in *Encyclopedia of Ocean Sciences*, edited by J. Steele, S. Thorpe and K. Turekian, pp. 3166–3173, Elsevier, New York.
- Marsh, B. D., and I. S. E. Carmichael (1974), Benioff zone magmatism, *J. Geophys. Res.*, 79, 1196–1206.
- Massoth, G. J., C. E. J. de Ronde, J. E. Lupton, R. A. Feely, E. T. Baker, G. T. Lebon, and S. M. Maenner (2003), Chemically rich and diverse submarine hydrothermal plumes of the southern Kermadec volcanic arc (New Zealand), in *Intra-*



- oceanic Subduction Systems: Tectonic and Magmatic Processes*, edited by R. Larter and P. Leat, *Geol. Soc. London Spec. Publ.*, 219, 119–139.
- Measures, C. I., J. C. Yuan, and J. A. Resing (1995), Determination of iron in seawater by flow injection analysis using in-line preconcentration and spectrophotometric detection, *Mar. Chem.*, 50, 3–12.
- Mortimer, N., and D. L. Parkinson (1996), Hikurangi Plateau: A Cretaceous large igneous province in the southwest Pacific Ocean, *J. Geophys. Res.*, 101, 687–696.
- Patterson, D. B., K. A. Farley, and B. I. A. McInnes (1997), Helium isotopic composition of the Tabar-Lihir-Feni island arc, Papua New Guinea, *Geochim. Cosmochim. Acta*, 61, 2485–2496.
- Resing, J. A., and M. J. Mottl (1992), Determination of manganese in seawater by flow injection analysis using online preconcentration and spectrophotometric detection, *Anal. Chem.*, 64, 2682–2687.
- Resing, J. A., and F. J. Sansone (1996), Al and pH anomalies in the Manus Basin reappraised: Comments on the paper by T. Gamo et al., “Hydrothermal plumes in the eastern Manus Basin, Bismark Sea: CH₄, Mn, Al, and pH anomalies,” *Deep Sea Res., Part I*, 43, 1867–1872.
- Resing, J. A., J. E. Lupton, R. A. Feely, and M. D. Lilley (2004), CO₂ and ³He in hydrothermal plumes: Implications for mid-ocean ridge CO₂ flux, *Earth Planet. Sci. Lett.*, 226, 449–464.
- Reyners, M., D. Eberhart-Phillips, G. Stuart, and Y. Nishimura (2006), Imaging subduction from the trench to 300 km depth beneath the central North Island, New Zealand, with *V_p* and *V_p/V_s*, *Geophys. J. Int.*, 165, 565–583.
- Schmidt, M. W., and S. Poli (1998), Experimentally based water budgets for dehydrating slabs and consequences for arc magma generation, *Earth Planet. Sci. Lett.*, 163, 361–379.
- Shor, G. G., H. K. Kirk, and H. W. Menard (1971), Crustal structure of the Melanesian area, *J. Geophys. Res.*, 76, 2562–2586.
- Smith, I. E. M., T. J. Worthington, R. B. Stewart, R. C. Price, and J. A. Gamble (2003), Felsic volcanism in the Kermadec arc, SW Pacific: Crustal recycling in an oceanic setting, in *Intra-oceanic Subduction Systems: Tectonic and Magmatic Processes*, edited by R. D. Larter and P. T. Leat, *Geol. Soc. London Spec. Publ.*, 219, 99–118.
- Stoffers, P., I. C. Wright, and Shipboard Participants (1999), Havre Trough–Taupo Volcanic Zone: Tectonic, magmatic and hydrothermal processes, in *Cruise Report R/V Sonne 135 Cruise, Ber. Rep. Ser. 1*, edited by P. Stoffers and I. C. Wright, 77 pp., plus appendices, Inst. für Geowiss., Univ. Kiel, Kiel, Germany.
- Stoffers, P., et al. (2006), Submarine volcanoes and high-temperature hydrothermal venting on the Tonga arc, southwest Pacific, *Geology*, 34, 453–456.
- Tamura, Y., Y. Tatsumi, D. Zhao, Y. Kido, and H. Shukono (2002), Hot fingers in the mantle wedge: New insights into magma genesis in subduction zones, *Earth Planet. Sci. Lett.*, 197, 105–116.
- Tatsumi, Y. (1989), Migration of fluid phases and genesis of basaltic magmas in subduction zones, *J. Geophys. Res.*, 94, 4697–4707.
- Turcotte, D. L., and G. Schubert (2002), *Geodynamics*, 456 pp., Cambridge Univ. Press, New York.
- Vogt, P. R., A. Lowrie, D. R. Bracey, and R. N. Hey (1976), Subduction of aseismic oceanic ridges: Effects on shape, seismicity, and other characteristics of consuming plate boundaries, *Geol. Soc. Am. Spec. Pap.*, 172, 59 pp.
- Wright, I. C., T. J. Worthington, and J. A. Gamble (2006), New multibeam mapping and geochemistry of the 30°–35°S sector, and overview, of southern Kermadec arc volcanism, *J. Volcanol. Geotherm. Res.*, 149, 263–296.
- Young, C., and J. E. Lupton (1983), An ultratight fluid sampling system using cold-welded copper tubing, *Eos Trans. AGU*, 64, 735.